



The 2022–2023 seismic sequence onshore South Evia, central Greece: evidence for activation of a left-lateral strike-slip fault and regional triggering of seismicity

Anna Serpetsidaki · Athanassios Ganas

Received: 30 November 2023 / Accepted: 19 March 2024 / Published online: 1 April 2024
© The Author(s) 2024, corrected publication 2024

Abstract On 29 November 2022, an earthquake of M_L 5.0 (M_w 4.8) occurred onshore South Evia Island (central Greece) preceded by a M_L 4.7 (M_w 4.6) event. The pattern of relocated aftershocks indicates the activation of a single, near-vertical fault segment, oriented NW-SE at shallow crustal depths (6–11 km). We suggest that both events ruptured a blind, left-lateral strike-slip fault, about 5 km southeast of

village Almyropotamos. We observed that a clear foreshock activity ($N=55$ events) existed before the two moderate events. The impact of the static stress loading on neighboring fault planes diminishes after a distance of 7 km from the November 2022 epicenters, where the static stress falls below +0.1 bar. We further explore triggering relationships between the 29 November events and the late December 2022 moderate events (M_L 4.9) that occurred about 60 km toward NW in the Psachna and Vlahia regions of central Evia. We present evidence of possible delayed dynamic triggering of the late December 2022 central Evia sequence, based on marked changes in seismicity rates and on measured peak ground velocities (PGVs) and peak dynamic strains, both exhibiting local maxima in their map distributions. The causes of the delayed triggering may be related to the well-known geothermal field in central/north Evia and the NW-SE strike of the seismic fault.

Highlights

- Relocation of the 2022–2023 seismic sequence in South Evia, Greece
- The 29 November 2022 events ruptured a blind, left-lateral strike slip fault striking NW-SE, previously unknown.
- The static stress transfer modeling indicated that stress loading on nearby faults can explain the occurrence of aftershocks for several months.
- Peak ground velocity distribution and seismicity rate changes may indicate delayed dynamic triggering of the late December 2022 sequences in central Evia by the November events.

Supplementary Information The online version contains supplementary material available at <https://doi.org/10.1007/s10950-024-10211-w>.

A. Serpetsidaki (✉)
Department of Geology, Seismological Laboratory,
University of Patras, 26504 Patras, Greece
e-mail: annaserp@upatras.gr

A. Ganas
Geodynamics Institute, National Observatory of Athens,
118 10 Lofos Nymfon, PO Box 20048, Athens, Greece
e-mail: aganas@noa.gr

Keywords Earthquake triggering · Relocation · Stress transfer · Evia · Central Greece

1 Introduction

South Evia Island is a low seismicity region of central Greece where no onshore strong earthquake record exists (Fig. 1; Papazachos and Papazachou 1997; Goldsworthy et al. 2002). An instrumental seismicity catalog with earthquakes of local magnitude $M4+$

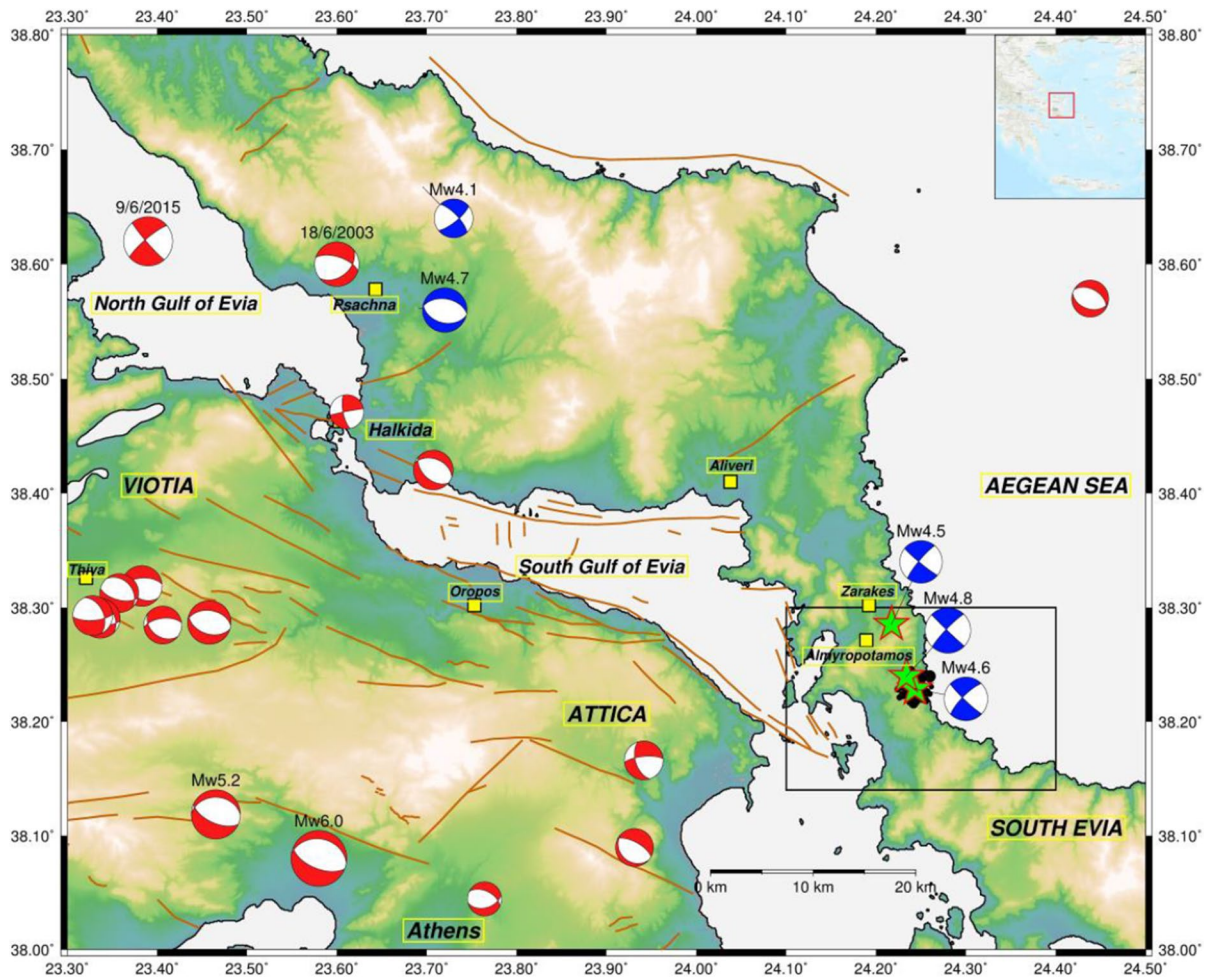


Fig. 1 Relief map of South Gulf of Evia region, central Greece. Beach balls indicate fault plane solutions of moderate seismic sequences since 1999 (red colors; source NOA). With blue beach balls, it is shown the 29 November 2022 (M_w 4.6– M_w 4.8), 28 December 2022 (M_w 4.7), 4 January 2023 (M_w 4.6– M_w 4.8), 22 April 2023 (M_w 4.5) events. Brown lines are active

faults from Ganas et al. (2013, 2023). The events with focal mechanism data are reported in Table S2. Focal mechanism for the 18 June 2003 event is from Benetatos et al. (2004). Focal mechanism for the 9 June 2015 event is from Ganas et al. (2016). Black box shows extent of Figs. 2, 3, 4. Inset box shows location of study area within Greece

for the period 1963–2003 shows no events $M_L > 5.0$ have occurred within a 50-km radius from South Evia (see supplementary Figure S1a and Table S1; data source: NOA). Evia is characterized by mountainous topography with a general NW–SE orientation, parallel to the strike of large normal faults that accommodate present day extension (Roberts and Jackson 1991; Roberts and Ganas 2000). The active normal faults control the geomorphology and they bound two Plio–Quaternary marine grabens (North and South Gulf of Evia; Fig. 1) whose asymmetry is evident in the topography, bathymetry, vertical movements of the

coastline and tilting of syn-rift sediments adjacent to them (e.g., Roberts and Jackson 1991; Perissoratis and Van Andel 1991; Pirazzoli et al. 1999; Cundy et al. 2010; Evelpidou et al. 2011; Valkanou et al. 2021; Caroir et al. 2023). Onshore syn-rift sequences are of Upper Miocene–Pliocene–Quaternary age (Mettos et al. 1991; Rondoyanni et al. 2007; Palyvos et al. 2006). The south part of the island is built with metamorphic bedrock (mainly schists and marbles; IGME 1991), carbonates, and a small Miocene–Pliocene basin (Kymi–Aliveri basin; Kokkalas 2001). While no large faults have been mapped onshore, it is

well known that several active faults occur offshore, inside the South Gulf of Evia (Papanikolaou et al. 1988; Perissoratis and Van Andel 1991) and on the Aegean side, south of the Island of Skyros (e.g., Stiros et al. 1992).

During October 2022–April 2023, a shallow earthquake sequence occurred onshore South Evia Island near the villages Zarakes and Almyropotamos (Fig. 1; Evangelidis and Fountoulakis 2023). The sequence initiated on 25 October 2022 (Fig. 1) with small size events that occurred in the vicinity of the main-shock, south of Almyropotamos (see Fig. 1 black dots) and has been peaked with a shock of magnitude $M_L = 4.8$ ($M_w = 4.6$) that occurred on 29 November 2022 04:32 UTC (event-1). This event was followed by a stronger $M_L = 5.0$ ($M_w = 4.8$) seismic event on the same day at 20:06 UTC (event-2), which was felt even in the city of Athens. Its seismic intensity reached V, according to the Institute of Engineering Seismology and Earthquake Engineering (ITSAK) measurements (Fig. S2) while only light damages were recorded in South Evia. During the following weeks many shallow aftershocks occurred, mostly onshore, while on 22 April 2023 08:38, UTC another moderate event $M_L = 4.5$ ($M_w = 4.5$; Fig. 1) occurred as well. Despite the moderate magnitude of the earthquakes and while intensity did not exceed V (Fig. S2), the sequence appeared to be interesting (from a seismotectonic point of view), driven by the fact that it took place in an area where no mapped fault existed on literature maps. Besides, previous seismic activity includes only a seismic swarm that occurred during 2003, at about 60 km to the north-west of the 2022–2023 sequence, near Psachna (Fig. 1; Benetatos et al. 2004; Papoulia et al. 2006). The background seismicity (considering shallow events with $M2.0+$) in both central and South Evia includes several hundreds of events scattered both onshore and offshore Evia (Fig. S1b, Fig. S1c; source <https://bbnet.gein.noa.gr/HL/databases/database>). Near the epicenters of the 2022 sequence, the occurrence of background events is mostly offshore, inside the South Gulf of Evia, as well as in NE Attica (see Fig. S1b).

In this study, we use regional seismological data to identify and characterize the seismic fault (location, kinematics, depth range) and its potential. The identification of an unknown fault is of key importance especially since the epicentral area neighbors populated towns of Evia Island and NE Attica but also lays

in a distance less than 50 km from the city of Athens; therefore, it could affect the regional seismic risk. We also use uniform-slip, near-vertical fault models to investigate the static stress transfer on receiver faults in South Evia and the neighboring crust. We further explore the variation of one strong motion parameter, the peak ground velocity (PGV) to assess the possibility of delayed dynamic triggering of two earthquake sequences, which took place at about 60 km to the NW, onshore central Evia (Fig. 1) respectively. The two latter sequences occurred in December 2022 and January 2023, motivating us to explore possible triggering relationships.

2 Tectonic setting

The island of Evia (also written as Euboea; Fig. 1) is located between the central Aegean region to the east and Attica–Viotia regions to the west (Fig. 1). The central Aegean mainly hosts fault segments of the right-lateral North Anatolian fault system and conjugate left-lateral faults (Papadopoulos et al. 2002; Karakostas et al. 2003; Ganas et al. 2005; Chatzipetros et al. 2013; Ganas et al. 2014; Karakostas et al. 2014; Papanikolaou et al. 2019). Attica forms the south margin of the E–W Quaternary rift of South Viotia–Oropos (Ambraseys and Jackson 1990; Goldsworthy et al. 2002; Ganas et al. 2005; Chousianitis et al. 2013; Grützner et al. 2016; Briole et al. 2021; Valkaniotis et al. 2023). Along the north coast of Attica, a set of parallel, north-dipping large normal faults accommodate NE–SW extension (e.g., IGME 1991; Grützner et al. 2016; Deligiannakis et al. 2018; Iezzi et al. 2021) which is also evidenced by Global Navigation Satellite System (GNSS) data (Chousianitis et al. 2013; Chousianitis et al. 2015; D’Agostino et al. 2020; Briole et al. 2021) and focal mechanism data (e.g., Kaviris et al. 2018; Konstantinou et al. 2020). These coastal normal faults of Attica face an opposing series of south-dipping normal faults that have been mapped along the southern coastline of Evia (Perissoratis and Van Andel 1991). The offshore area (i.e., between Attica and South Evia) is seismically active in the depth range 5–20 km (Papoulia et al. 2006; Konstantinou et al. 2020). Further evidence for a full-graben structure regarding the South Gulf of Evia rift has been suggested by Rondoyanni

et al. (2007) for the region to the SE of town of Halkida (Fig. 1).

Further northwest, an active deformation component of left-lateral shear was identified for the first time inside the North Gulf of Evia rift from seismological data (Ganas et al. 2016). The seismological data provided evidence that on 9 June 2015 event 01:09 UTC a left-lateral, NW-SE striking, near-vertical fault, ruptured at mid-crustal depths (~10-km) about 15 km NW of Halkida (Fig. 1). The left-lateral shear faulting inside the Gulf of Evia is kinematically compatible to the ongoing NNE-SSW extension (N14°E; Roberts and Ganas 2000) accommodated by moderate to high-angle normal faults. In addition, inside the north gulf of Evia several E-W to NW-SE minor normal faults exist (Sakellariou et al. 2007; Karastathis et al. 2007; Caroir et al. 2023) that are interpreted as secondary structures with moderate seismic potential. As both rifts (North and South Gulf of Evia) are of similar Plio-Quaternary age (Roberts and Jackson 1991; Roberts and Ganas 2000; Goldsworthy et al. 2002), it may be expected that similar, left-lateral shear faults occur at mid-crustal depths, with moderate seismic potential.

Across the south gulf of Evia estimates of tectonic strain from Global Navigation Satellite System (GNSS) data (Chousianitis et al. 2013; Chousianitis et al. 2015; D'Agostino et al. 2020) indicate NNE-SSW extension. The rate of extension ranges from 1.2 mm/year (equivalent to 1-D strain rate of 23.2 ns/year) to 0.6 mm/year (13 ns/year) toward the southern termination of the rift. While the main component of the deformation is extensional, the occurrence of left-lateral shear inside the North Gulf of Evia (Ganas et al. 2016) points out that a similar slip component may be active inside the South Gulf. The occurrence of the 2022–2023 sequence gave us the data necessary to examine the kinematics of the mainshock and identify its nature.

3 Data and methods

3.1 Relocation of seismicity

We study the seismicity sequence in South Evia (Central Greece) between the 25th of October 2022, when the first moderate events occurred, and the 23rd of April 2023. The sequence was recorded by the

broad-band and strong motion stations of the regional Hellenic Unified Seismic Network (HUSN) stations and broad-band stations of the AdriaArray project (a new European geophysical initiative; Kolínský et al. 2022), as well (Fig. S3). P- and S- arrival times used in this study were manually picked by the Geodynamics Institute of the National Observatory of Athens (GI-NOA).

The sequence includes about 800 seismic events with magnitude M_L between 0.5 and 5.0, which were initially located using the HYPOINVERSE code (Klein 2002). Several velocity models were examined during the location–relocation procedure such as Konstantinou (2018), Konstantinou et al. (2020), Mouzakiotis and Karastathis (2016) and Kaviris et al. (2007) (Fig. S4). The comparison was initially performed on the HYPOINVERSE results including the determination of location errors (Fig. S5) and the epicenters' distribution (Fig. S4). The crustal model of Kaviris et al. (2007) was finally selected since it depicted the lowest errors and has been derived from a recent seismic experiment including the district of the study area (Fig. S5). The average absolute location errors reported by HYPOINVERSE where mean rms (root mean square) travel time error 0.14 s, ERH=0.61 km, and ERZ=0.95 km for horizontal and vertical uncertainties, respectively. The value of V_p/V_s ratio was set to 1.75 according to the Wadati diagram results (Fig. S6). The applied distance weighting was set to nullify the influence of stations at epicentral distances further than ~120 km.

In order to improve the initial events' locations, the double difference relocation HypoDD (Waldhauser 2001) procedure was performed. HypoDD determines relative locations within clusters, using a double difference algorithm, developed by Waldhauser and Ellsworth (2000). It improves relative location accuracy by strongly reducing the influence of the velocity structure on locations and uncertainties caused by arrival time readings errors, by minimizing the double-difference between observed and calculated travel times through iterative weighted least squares using the conjugate gradients method. The relocation procedure takes into account both waveform cross-correlation and catalog differential travel time data to provide an enhanced picture of the seismic activity.

Waveform cross-correlation was incorporated in the relocation procedure, for the closest 21 stations (distance <75km, Fig. S3), in order to enhance the

strong correlated events by decrease of the relative location uncertainties induced by the P- and S-wave arrivals picking inaccuracies. Full signal waveforms were cropped in windows containing both P and S waves, filtered between 2 and 6 Hz, and a threshold of 70% was set concerning the waveform coherency. The double-difference residuals for the pairs of earthquakes at each station were minimized by weighted least squares, using the method of conjugate gradient least squares (LSQR). Errors reported by LSQR are grossly underestimated and need to be assessed independently by using the singular value decomposition technique (SVD) on a subset of events (Waldhauser and Ellsworth 2000). Therefore, in a first step, a subset of the sequence, including the strongest events ($M_L > 3$), was relocated using the SVD method (Fig. S7) indicating onshore activity-oriented NW-SE. A good data fit of mean rms < 0.12s was obtained. Next, the LSQR scheme was followed for the total dataset including data from stations in a maximum distance of 75km (Fig. S3; this distance includes SKY station to the North to reduce the azimuthal gap). The velocity model used in the relocation was the model used in the initial location process. Variations in station distribution for each event pair can introduce errors in relative event locations that cannot be quantified directly (Waldhauser and Ellsworth 2000). We apply the jack-knife method (e.g., Efron 1982) to estimate the variance of errors in each coordinate direction.

The procedure involves repeated relocation, each time sub-sampling the data by deleting one station at a time. No outliers are removed during this process. The mean and median absolute perturbation on each direction (Table 1) and the 95% confidence interval ellipsoids (Fig. S8) are then determined from the distribution of the perturbed hypocenter positions for each event. The majority of the events are described by a small error ellipsoid (less than 1 km; Fig. S8) which indicates that the relevant relocated positions are robust. The HypoDD final results include 88% of the initial dataset (701 events) (rms residual for cross-correlated data: 0.22 s, rms residual for catalog data: 0.16 s, Fig. S9).

3.2 Focal mechanisms

The moment tensor (MT) solutions of the strongest events were calculated by GI-NOA (<https://bbnet.gein.noa.gr/HL/seismicity/mts>), yet to confirm the source of the weaker events the MT inversion was performed for the three weaker aftershocks (M_w between 3.5 and 3.9) of the sequence (Table 2, Fig. 2). The ISOLA platform was employed (for detailed description see Sokos and Zahradnik 2008; Zahradník and Sokos 2018). Complete waveforms were used, without separation of individual phases; full-wave Green’s functions were calculated by the discrete wavenumber method (Bouchon

Table 1 Statistics from the station jack-knife test of relocation robustness

Mean dx (m)	Mean dy (m)	Mean dz (m)	Median dx (m)	Median dy (m)	Median dz (m)	std dx (m)	std dy (m)	std dz (m)
124.9	156.3	267.5	61.9	93.6	201.1	205.7	187.5	268.3

Table 2 Moment tensor solutions calculated in this study and by GI-NOA (*)

Origin yymmdd_hh:mm	Centroid latitude (°)	Centroid longitude (°)	Centroid depth (km)	Strike p1/p2 (°)	Dip p1/p2 (°)	Rake p1/p2 (°)	MomentMo (Nm)	Mw
20221129_04:32*	38.2701	24.2793	9.0	134/225	84/77	-13/-174	9.638e+15	4.6
20221129_20:06*	38.2616	24.1703	9.0	134/224	88/83	-7/-178	1.778e+16	4.8
20221203_10:35	38.2600	24.2400	6.0	316225/	86/80	10/176	3.923e+14	3.7
20221203_10:51	38.2330	24.2479	8.0	130/221	85/80	-10/-175	6.531e+14	3.9
20221209_00:06	38.2600	24.2600	8.0	135/225	85/88	-2/-175	2.144e+14	3.5
20221214_15:28*	38.2662	24.2112	11.0	131/221	88/82	-8/-178	3.268e+15	4.3
20230422_08:38*	38.2854	24.2172	8.0	130/220	85/82	-7/-175	7.086e+15	4.5

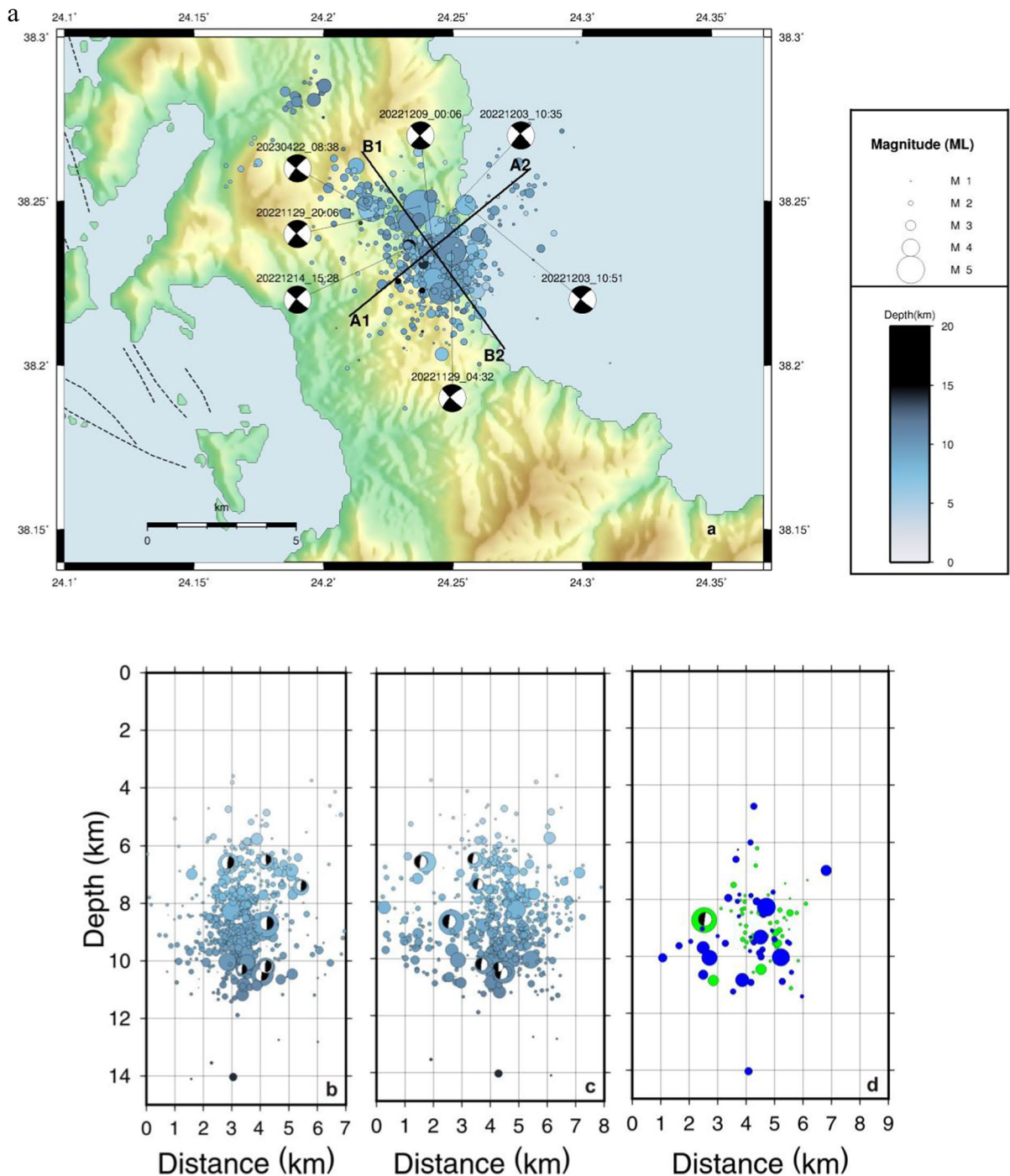


Fig. 2 **a** Map showing the spatial distribution of the relocated (HypoDD) sequence (see also Fig. S10a for a plot with transparent, depth-free, events). The MT solutions (Table 2) are plotted as beach balls (The shaded quadrants indicate compression and the light quadrants indicate extension). **b**, **c**, **d** Distribution of the relocated (HypoDD) sequence at cross-sections A1-A2 (**b**) and B1-B2 (**c**), corresponding to Fig. 2.a. Notice

the near-vertical structure (about 2 km wide) that is visible in the left panel (i.e., across strike). The length of the structure is about 6 km (middle panel). **d** Additional projection of the cross-section B1-B2, where green and blue colors indicate the foreshocks and aftershocks of event-1 (MT is shown) respectively

1981). The 1D velocity model suggested by Kaviris et al. (2007) and the ratio V_p/V_s value 1.75 were adopted. The inversion was performed in the frequency bands 0.04–0.09 and 0.06–0.12 Hz, depending on the magnitude of the event and the distance from the station used.

The results are expressed in terms of the double-couple component of the deviatoric solution, represented by the scalar moment, strike, dip, and rake. Several HUSN network broadband stations (ATH, SKY, THVA, MRKA, KARY) were considered in the process. The variance reduction (VR) was >60% in all three cases, while the double-couple (DC) percentage was >70% (Fig. S11). The quantification of the focal mechanism variability in FMVAR is done via the use of Kagan angle (i.e., the minimum rotation angle between two P-T-N coordinate systems describing the focal mechanisms under comparison). The angle can vary from 0° (perfect agreement between two solutions) to 120° (total disagreement), the values below 20°–40° indicate a good agreement. For more details and references,

see paper by Sokos and Zahradnik (2013). In our study, FMVAR values were between 12° and 18°.

3.3 Parameters of the earthquake sequence

The seismic sequence debuted in Evia Island on October 25 and 26, 2022, and was followed by 55 events until late November 2022 (Fig. 4). The seismicity seemed to pause until November 28, when limited number of events took place, while during the November 29th, the two major events (M4.6 & M4.8) occurred. Throughout the next days, the seismic sequence showed a temporal decay until the 3rd of December 2022, when a stage with several events of magnitude $M_L > 3.0$ initiated (Figs. 3, 4). Next, on April 22, 2023, another moderate event ($M_w = 4.5$) occurred, followed by several weak events while during the next days the seismicity demonstrated some degradation.

The Z-map package (Wiemer 2001) has been applied for obtaining the characteristics of the sequence such as the cumulative number of events with time (Fig. 5). We also studied the frequency–magnitude distribution of the

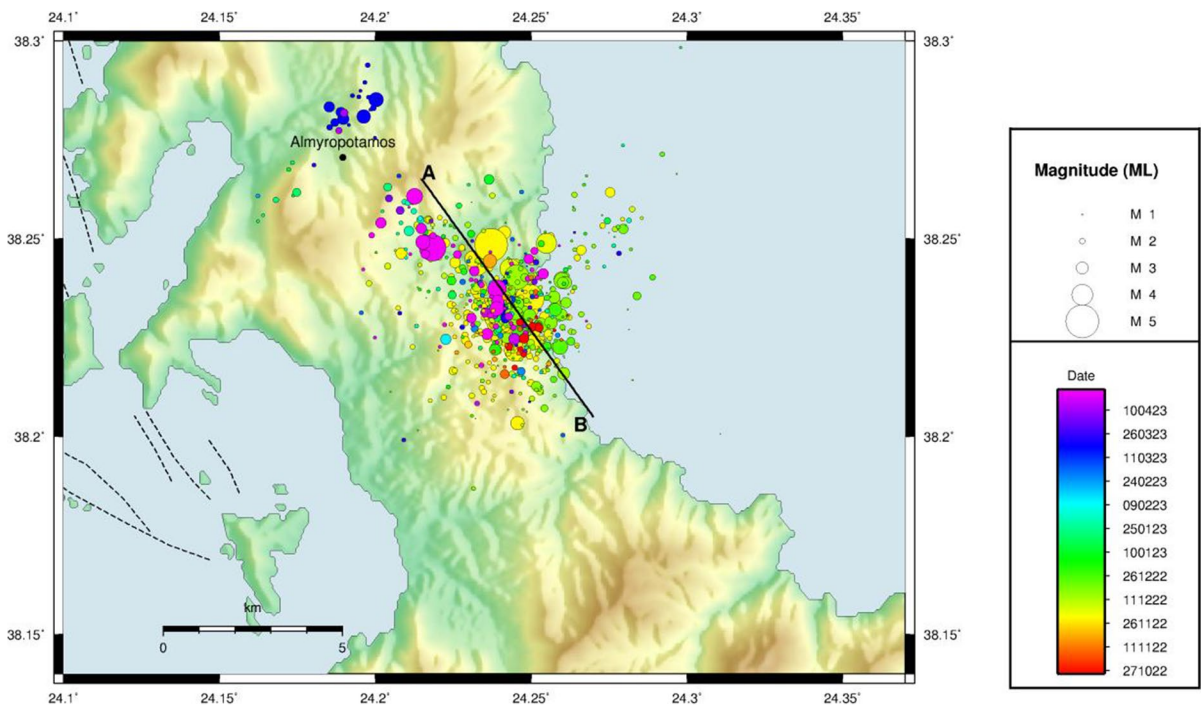


Fig. 3 Map of South Evia showing the time distribution of the relocated sequence events colored according to time of occurrence for the time period 25 October 2022–23 April 2023. Date

on color scale is formed as DDMMYY. Thick black line indicates line of projection of events shown in Fig. 4

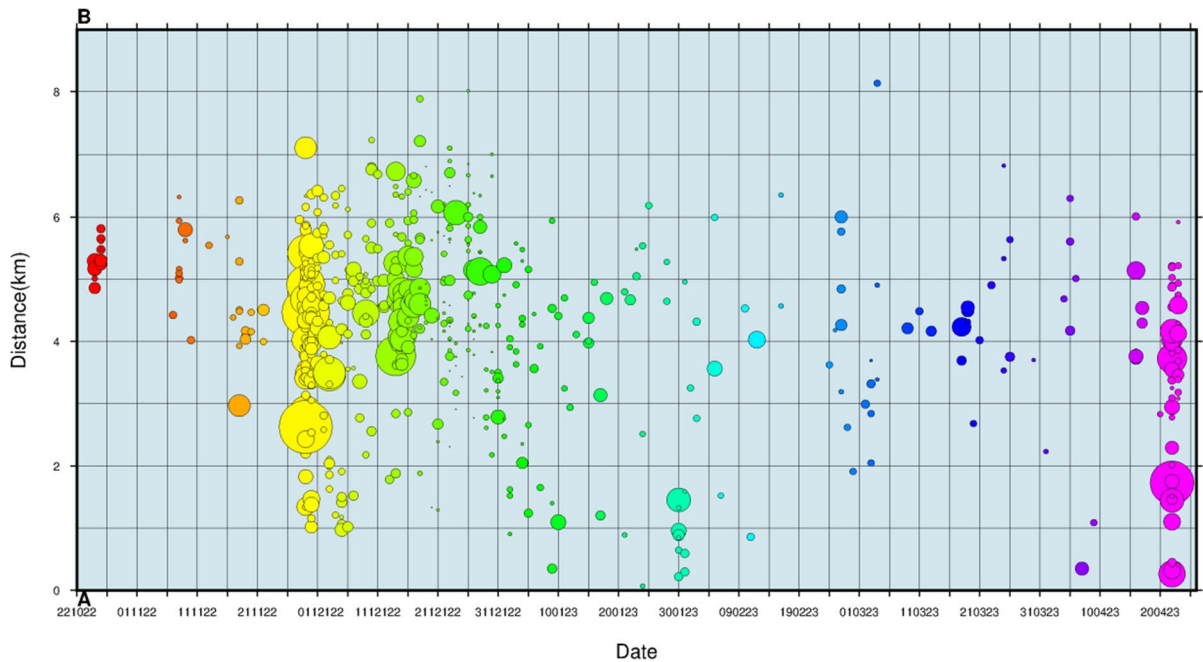


Fig. 4 Space-time evolution of the South Evia sequence projected along a 10-km section AB (thick black line in Fig. 3), for the time period 25 October 2022–23 April 2023. The color scale is the same as in Fig. 3

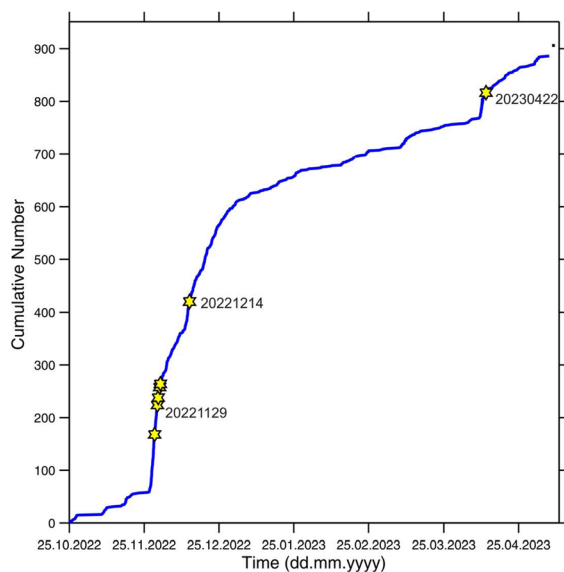


Fig. 5 Frequency-time evolution of the sequence for the time period 25 October 2022–24 May 2023 (extended period is plotted to demonstrate the sequence decay). Yellow stars denote the major events with $M_L > 4.0$

2022–2023 earthquakes. The estimation of the completeness magnitude (M_c) is a required step for any seismic sequence study. This magnitude, M_c , is the minimum magnitude above which all events are reliably detected in a defined region and time. This is crucial for further seismicity analysis, given that a magnitude lower than M_c leads to biased results (Rydelek and Sacks 1989; Kagan 2004; Mignan et al. 2011; Olasoglu et al. 2016). Wiemer and Wyss (2000) assessed the minimum magnitude for complete earthquake data. Then, parameters a , b were computed with a Maximum likelihood solution method for 55 events (foreshocks) of the period 25.10.2022–28.11.2022 (blue color) and the main sequence period, 29.11.2022–23.4.2023 (green color); the graph is depicted in Fig. 6.

4 Earthquake interaction

4.1 Static triggering and relation to aftershock patterns

It is well established that the coseismic slip along the fault plane causes changes in static stress patterns that may trigger subsequent earthquakes on

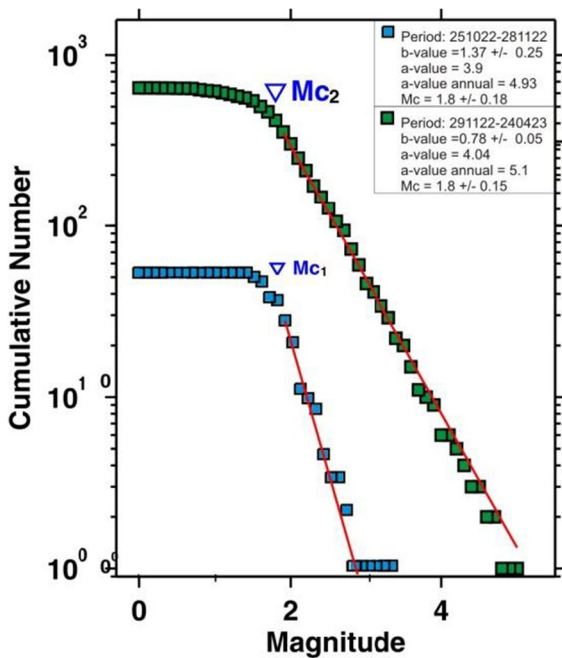


Fig. 6 Frequency–magnitude graph showing maximum likelihood solution for the seismic sequence period 29.11.2022–23.4.2023 (green color) b -value=0.78(+/-0.05), and the foreshock sequence period 25.10.2022–28.11.2022 (blue color) with b =1.37 (\pm 0.25). The magnitude of completeness $M_c = 1.8$ is the same in both cases

neighboring segments as well as aseismic slip on unruptured patches of the seismic fault itself (e.g., Lin and Stein 2004; Ganas et al. 2006; Atzori et al. 2008; D’Agostino et al. 2012; Kassaras et al. 2022). In this context, it is important for hazard assessment to identify other possible faults in the broader Evia region that may have been brought closer to failure by the stress changes associated with the 2022 South Evia earthquakes. To investigate the Coulomb stress variations, we calculated the Coulomb stress change (Coulomb Failure Function, CFF, or Coulomb stress; Reasenbergs and Simpson 1992), induced by the mainshock using our fault model (Table 3). We assume a rectangular dislocation model with a uniform-slip size of 3 by 3 km constrained by the cross-sections of the relocated seismicity, including the extent of aftershocks (Fig. 2). We consider as source for the M4.6 strike-slip event-1 the dimension of a single slip patch, provided by the empirical relationship of Wells and Coppersmith (1994): $\log RA = a + b \times M$ (where $a = -3.42$ and $b=0.9$; RA is rupture area) for strike

Table 3 Parameters of fault models for event-1 (29 November 2022 04:32 UTC) and event-2 (29 November 2022 20:29 UTC) used in Coulomb stress modeling, respectively

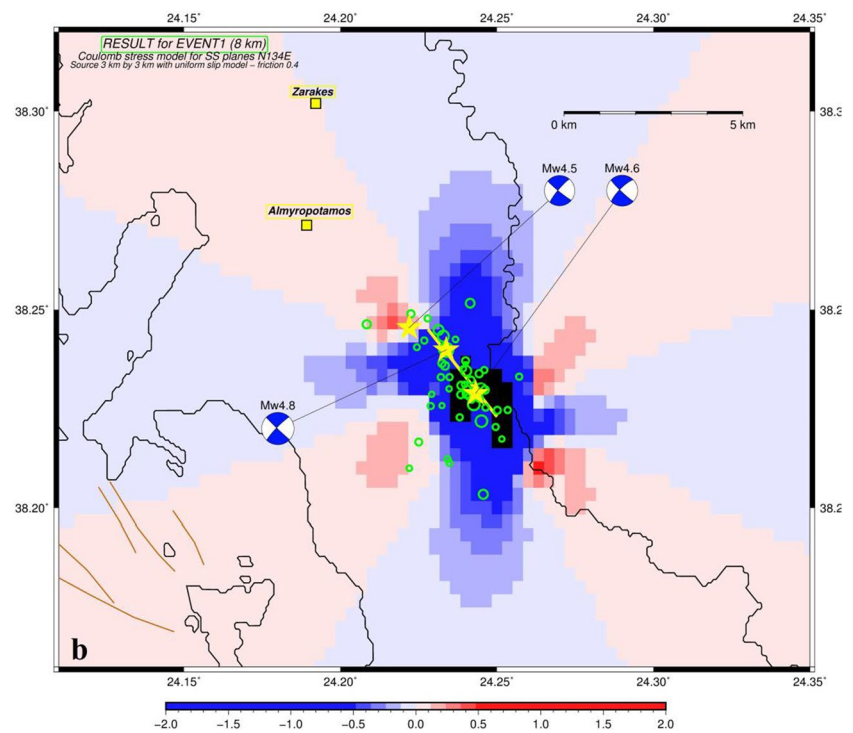
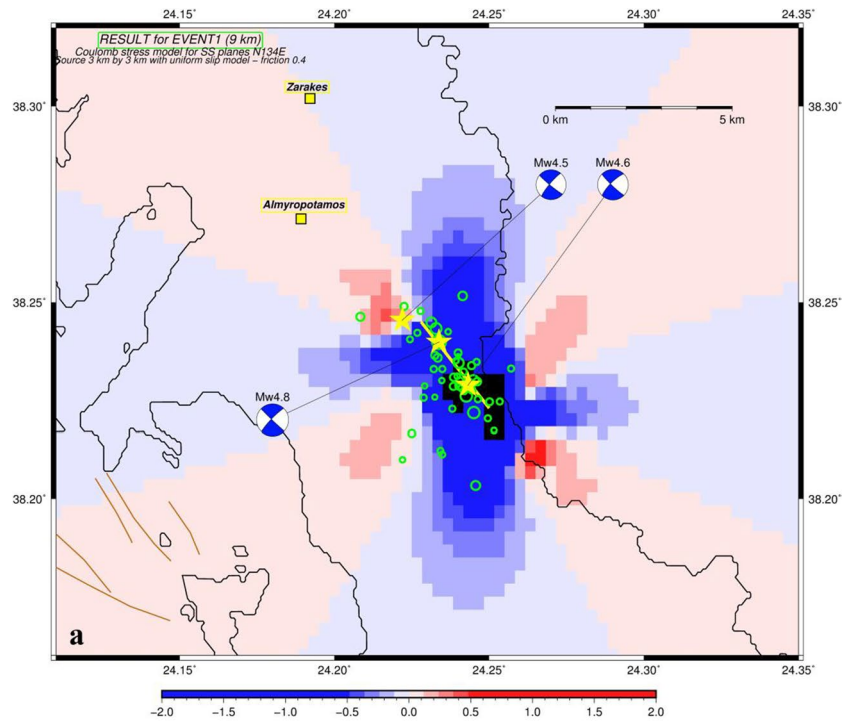
Parameter	Event-1	Event-2
Centroid latitude (°)	38.2288	38.2398
Centroid longitude (°)	24.2432	24.2337
Depth, km	9	8
Magnitude: M_w (NOA)	4.6	4.8
Fault strike (°)	134	134
Fault dip angle (°)	84	88
Rake of slip-vector (°)	-12	-6
Fault length (L), km	3	3
Fault width (W), km	3	3
Uniform slip (SS), m	0.03	0.07
Uniform slip (DS), m	0.007	0.007

slip faults. This formula provides a $RA = 5.24 \text{ km}^2$ for a M4.6 source and 7.94 km^2 for a M4.8 source (event-2), respectively. Given the uncertainties associated with regression statistics and the moderate size of the events, we considered as source dimension a square patch of $3 \times 3 \text{ km}$ (or 9 km^2). A 3-km size for fault length seems a suitable approximation given that the distance between the epicenters of the two events is less than 2 km (Fig. 2) while the hypocentral depths are at 8 km (event-2) and 9 km (event-1).

First, we calculate the Coulomb stress change due to rupture on event-1 on fault segments with the same kinematics and geometry (Fig. 7) at the depth range 8–9 km, and assuming an effective friction coefficient $\mu' = 0.4$, as is commonly used in stress interaction studies (e.g., Harris and Simpson 1998; Freed 2005). The Coulomb stress change was computed in an elastic half space (Okada 1992) by assuming a shear modulus of $3.0 \times 10^{10} \text{ Pa}$, Poisson’s ratio 0.25. The parameters of the two fault models are given in Table 3 using the MT determinations of this study (Table 2).

The Coulomb stress change patterns form both along- (i.e., N134°E) and across-strike positive stress lobes (red color in Fig. 7); however, most of the event-1 aftershocks occur in negative (relaxed) stress areas (or stress shadows, Harris and Simpson 1998; see a cross-section orthogonal to fault’s strike in Fig. S11 for a depth distribution). This is probably caused by the assumption that coseismic slip was uniformly

Fig. 7 Map of Coulomb stress computed on left-lateral receiver faults striking N134°E due to event-1, at 9-km depth (a) (see Fig. S12 for a stress cross-section at right-angles to the causative fault.) and 8-km depth (b). Color palette of stress values is linear in the range -2 to $+2$ bar (1 bar=100 kPa). Blue areas indicate unloading, red areas indicate loading, respectively. Black color shows the area where stress reduction was < -2 bar. Green circles are aftershocks between 04:32 and 20:29 UTC. Note that the aftershocks are aligned NW-SE parallel to the strike of the 1st rupture (yellow line)



distributed along the fault plane and/or that some of off-fault aftershocks occurred on fault planes exhibiting different kinematics than those of event-1. However, most of the event-1 aftershocks are oriented NW-SE in map-view (i.e., similar orientation to the modeled fault plane) and they are located ± 1 km from the fault (Fig. 7) so it is reasonable to assume that they may be co-planar to event-1 (i.e., on-fault aftershocks). The hypocenter of event-2 is located about 2 km to the NW of event-1 at a depth of 8 km; therefore, it may have been triggered by Coulomb stress transfer as expected; however, it is not confirmed because of the modeling limitations (the uniform slip assumption includes the hypocentral area of event-2; Fig. 7b).

Next, we calculated the stress changes due to event-2 (29 November 2022 20:29 UTC; $M_w=4.8$). At 8-km depth the lobe pattern is similar to that of event-1 except for the amplitudes of transferred stress that are larger (Fig. 8). Two large lobes with negative stress levels (stress shadows) have formed in a N-S direction. Most aftershocks of both events occurred to the southwest of event-2 epicenter, while many events occurred inside the stress shadows. Several active faults inside the South Gulf of Evia were loaded with Coulomb stress less than 0.1 bar. The impact of the stress loading on target planes diminishes after a distance of 7 km from the epicenter of event-2, where the static stress falls below +0.1 bar. The events of the 22–23 April 2023 seismic burst occurred on either side of the M4.8 event (yellow circles in Fig. 8). The M4.5 aftershock occurred about 1.5 km NW of the M4.8 event (event-2).

We also modeled static stress transfer patterns due to event-2 resolved on optimal planes to regional extension. We used the extension direction found by Chousianitis et al. (2015) based on GNSS data, that is N18°E for this area of South Evia (we used the grid node located 13 km to the NE of the 2022 events). A similar strain axis orientation (NNE-SSW) was obtained by D'Agostino et al. (2020) and Konstantinou et al. (2020). The stress pattern (at 8-km depth) shows positive lobes to the SE of the epicenter of event-2 where many aftershocks are located (Fig. 8). The loading of this area reached levels greater than +2 bar (Fig. 8) and this may justify the occurrence of aftershocks for several months (end of April 2023; see time plot in Fig. 4). We attribute the occurrence of off-fault aftershocks inside the stress shadows to

the uniform-slip assumption along the fault plane, used also in the CFF modeling due to 2nd rupture. Nevertheless, the uniform slip model may explain the overall NW-SE arrangement of off-fault aftershocks (Fig. 8). Similarly to the specified target faults case, the static stress loading falls below 0.1 bar at distances larger than 7 km from the mainshock.

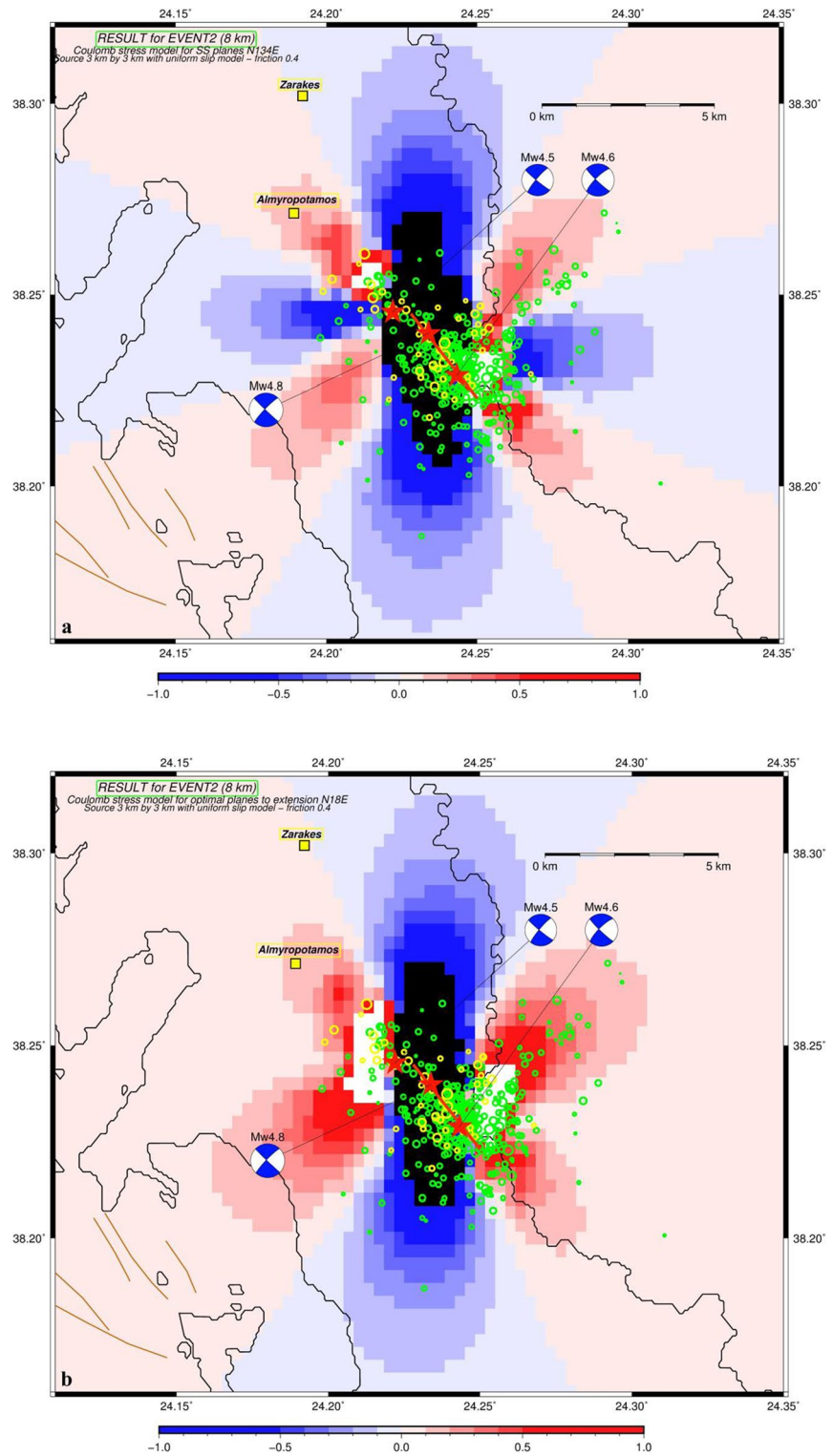
5 Discussion

5.1 Seismotectonic setting and left-lateral shear onshore South Evia

In this section, we discuss our seismological findings from a very comprehensive investigation of the source of 29 November 2022 Mw 4.6 and 4.8 earthquakes along a blind, strike-slip fault onshore South Evia Island. This seismic sequence occurred in a critical area, a few km to the east of a marine graben (i.e., South Gulf of Evia), which hosts active faults capable of generating potentially large ($M > 6$) earthquakes (i.e., Goldsworthy et al. 2002; Grützner et al. 2016; Deligiannakis et al. 2018; Iezzi et al. 2021).

The majority of the relocated events of 5-months long period, are distributed in a dense cluster, onshore South Evia (Fig. 2.a, Fig. S10a) indicating the activation of the NW-SE striking fault plane at shallow depths ($h < 12$ km, Fig. 2.a, b). The spatial distribution shown in the cross sections A1-A2 (across-strike) and B1-B2 (along strike; Fig. 2.b, c) reveals that the relocated hypocenters form an almost vertical structure, in depth between 6 and 11.5 km. The structure appears coherent with focal mechanisms (Table 2) of the major events (strike N134°E, dip 88°). Furthermore, we applied the HC method (Zahradnik et al. 2008) in order to identify which of the nodal planes, obtained by the MT solution, is the causative fault (Fig. S10b and c); the results support the NW-SE nodal plane. Moreover, the additional solutions reveal that even the weaker events, which occurred a few days later than the 29 November events, are also attributed to strike-slip movement source like the stronger events. As indicated by the relocated seismicity data, there is a single causative fault, while its overall rupture zone dimensions are about 6×6 (km²). The overall picture of the relocated aftershocks pattern indicates the activation of a single, left-lateral, near-vertical

Fig. 8 **a** Map of Coulomb stress computed on left-lateral receiver faults striking N134°E due to event-2, at 8-km depth. **b** Map of Coulomb stress computed on optimally oriented faults to regional extension N18°E due to event-2, at 8-km depth. Color palette of stress values is linear in the range -1 to $+1$ bar ($1 \text{ bar} = 100 \text{ kPa}$). Blue areas indicate unloading, red areas indicate loading, respectively. Black color shows the area where stress reduction was < -1 bar and white color areas where stress increase was > 1 bar. Green circles are aftershocks between 29 November 20:29 UTC and 28 December 2022. Red line indicates the surface projection of the modeled, left-lateral seismic source. Yellow circles represent events of the April 22–23 seismic burst



fault segment hosting the two major shocks of the sequence (see Fig. 2), as well as the 22 April 2023 M4.5 event. Certain events located in a distance, toward NE, may indicate the existence of another structure (described by Evangelidis and Fountoulakis 2023), which is not well illustrated. Finally, few events to the NNW are not connected to the main cluster and may belong to the activation of small faults.

The results of the space–time analysis showed that until the 12th of December 2022, the sequence demonstrated decay, yet after the 14th of December 2022, the seismicity rate shows some recovery (Fig. 5). Moreover, while the sequence evolution until 22 of April 2023 exhibited certain decay, the occurrence of the Mw4.5 event seemed to initiate a new stage. The spatial distribution of the seismic events (Fig. 3) does not reveal any migration of the seismicity, to a different epicentral area in South Evia, although a small number of events are located more distant from the cluster's center. The evolution of the sequence, as seen in Fig. 5, implies that it was still in progress until 23 April 2023 and aftershocks were still expected; an extended look until May 2023 shows that the seismicity rate tended to stabilize. The overall assessment of this sequence includes a series of shallow events occurring within a rupture zone of about 6-km long (Fig. 2), oriented NW-SE onshore South Evia. Most of the events show an almost uniform distribution except for the last period (2023) where most of the earthquakes have occurred toward the NW part, i.e., near Almyropotamos (Figs. 3, 4). In comparison to Evangelidis and Fountoulakis (2023) findings, we confirm the NW-SE orientation of the causative fault, yet we note that the distribution of epicenters in our study suggests that the seismic fault is mostly located onshore; During the testing of different velocity models (see also Sec. 3.1), we observe significantly higher residuals for the model by Konstantinou et al. (2020) that was used for the relocations in the study by Evangelidis and Fountoulakis (2023). This discrepancy may explain the difference in resulting event locations compared to their study.

Moreover, the statistical analysis shows that the b -value of the foreshocks is notably higher than that of the aftershocks (1.37 vs. 0.78). Despite the relatively low value of the b -parameter of the population of aftershocks (0.78), we note that a comparable b -value=0.86 was obtained by Karakostas et al.

(2014) for the aftershock sequence of the 2013 N. Aegean Sea earthquake.

5.2 Foreshock activity patterns

During the seismicity period October–November 2022, we identified 55 events as foreshocks (Fig. 9) including an event $M_L=3.2$ on 18 November 2022 and an $M_L=3.3$ event on 28 November 2022. The foreshock events occurred within 35 days before the 29 November 2022 mainshock with local magnitude between 1.4 and 3.3. Most foreshocks (55) occurred within 1-km radius from the epicenter of the 29 November 2022 04:32 UTC event. The foreshock activity started on 25 October 2022, 35 days before the mainshock and fits the pattern of other sequences in Central Greece where such sequences originate within four months from the mainshock (e.g., Papadopoulos et al. 2000). The 2022 foreshocks occurred in a sequence of two groups (25–26 October, 10–22 November), the last one 7 days before the mainshock (see Fig. 4 for a time evolution plot of the events). The occurrence of foreshocks around the hypocenter of event-1 (Fig. 9; Fig. 2.d) favors a cascade-up model (i.e., Ellsworth and Bulut 2018) for the nucleation of event-1, where the sequence of foreshocks builds up both temporally (Fig. 5) and spatially (Fig. 2d and Fig. 9) around the hypocenter of the forthcoming mainshock. Moreover, by examining the catalog ~ 1.0 h before the $M_L=4.8$ event, we confirm that six (6) immediate foreshocks were observed. The foreshocks also appear to fit better a NW-SE arrangement although the scatter is considerable. Furthermore, the frequency-magnitude distribution of the foreshocks is notably different than the post-mainshock sequence as the foreshock b -value = 1.37 vs. 0.78 (see plot in Fig. 6). The relatively large b -value of the foreshock sequence may indicate relatively low differential stress level in the upper crust (Scholz 1968; see Fig. 4 for depth distribution), or it may be related to high fluid pressure associated with geothermal fluids that are known to exist at shallow levels in South, central and North Evia (e.g., Karastathis et al. 2011; Kanellopoulos et al. 2016). The distribution of the geothermal fields near Halkida (Fig. 1; Lilantio Pedio) is described by Kavouridis and Papadeas (1990), Hurter and Schellschmidt (2003), and

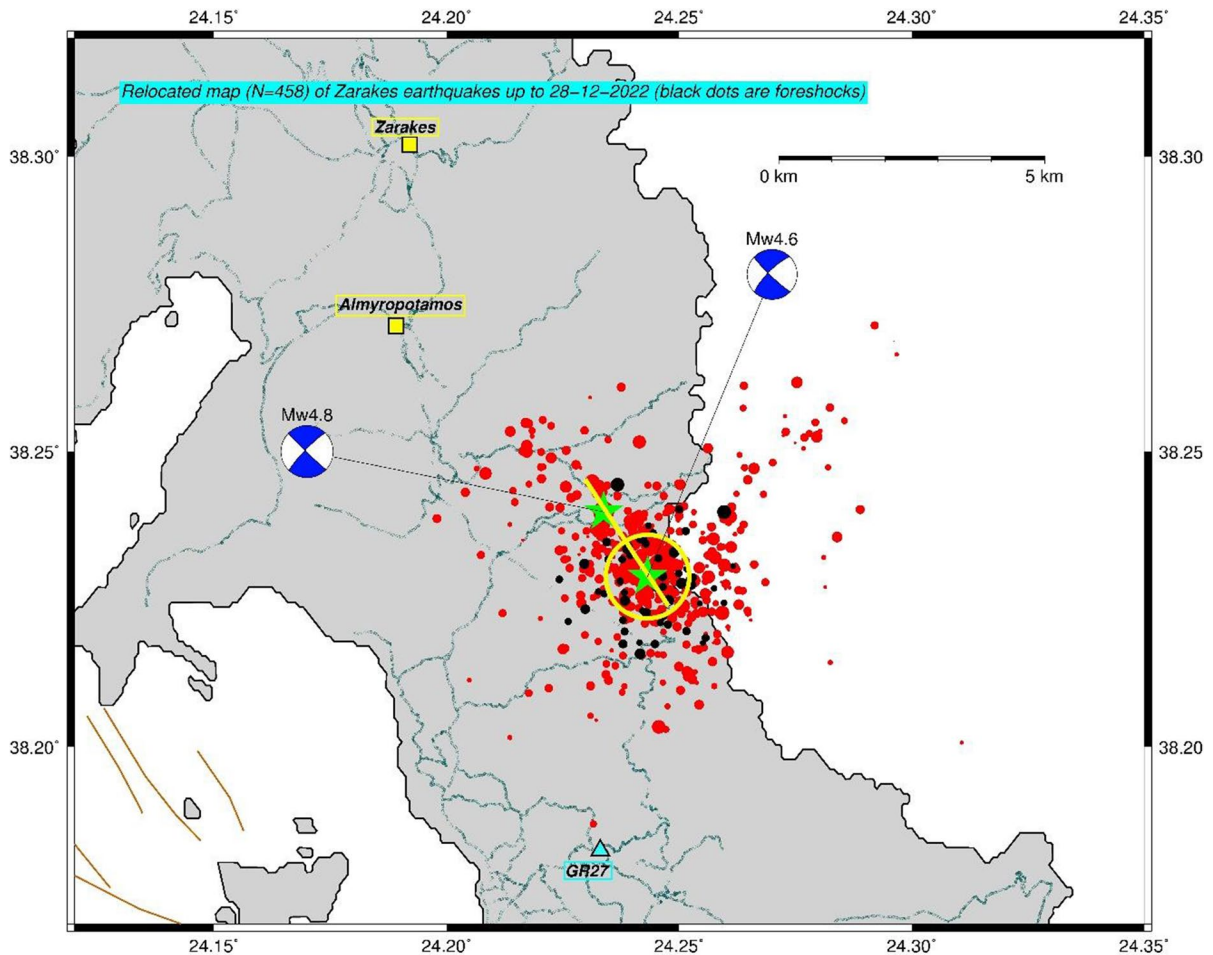


Fig. 9 Map showing relocated epicenters of the 2022 South Evia sequence including foreshocks (black dots). The yellow circle indicates 1-km distance from the epicenter of event-1.

Thick yellow line indicates surface projection of the seismic fault. Beach balls indicate focal mechanisms of main events (lower hemisphere projections)

Karytsas et al. (2019), while Tombros et al. (2021) studied the association between fault orientation and the flow of the hydrothermal fluids in Kallianos (South Evia) area. We thus documented that a clear foreshock activity existed before the two moderate, intraplate events.

5.3 Dynamic triggering of the central Evia events

After the earthquakes of November 2022, two short sequences were initiated about 60-km to the NW in central Evia (Fig. 10; Psachna and Vlahia regions). The sequence A started with a $M_L=4.9$ event (the major one) on 28 December 2022 and lasted until January 2023,

while the sequence B began on 4 January 2023 with a $M_L=4.2$ event (the major one) and lasted until the end of January (Fig. 10, Fig. S13). These events occurred over a distance several times the dimensions of the 29 November 2022 mainshock fault rupture (3 by 3 km; Fig. 9). The central Evia (Psachna; area A) sequence occurred inside a region which was nearly dormant for 20 years, since June 2003 (see Fig. 1). Inspection of the seismic catalogs (Table S1 and Fig. S1a, b, c) reveals that there were not any events $M_L \geq 4.3$ located in areas A and B from July 2003 to December 2022. We suggest that this timing may not be coincidental but that the two sequences of central Evia are related to the main one of the South Evia.

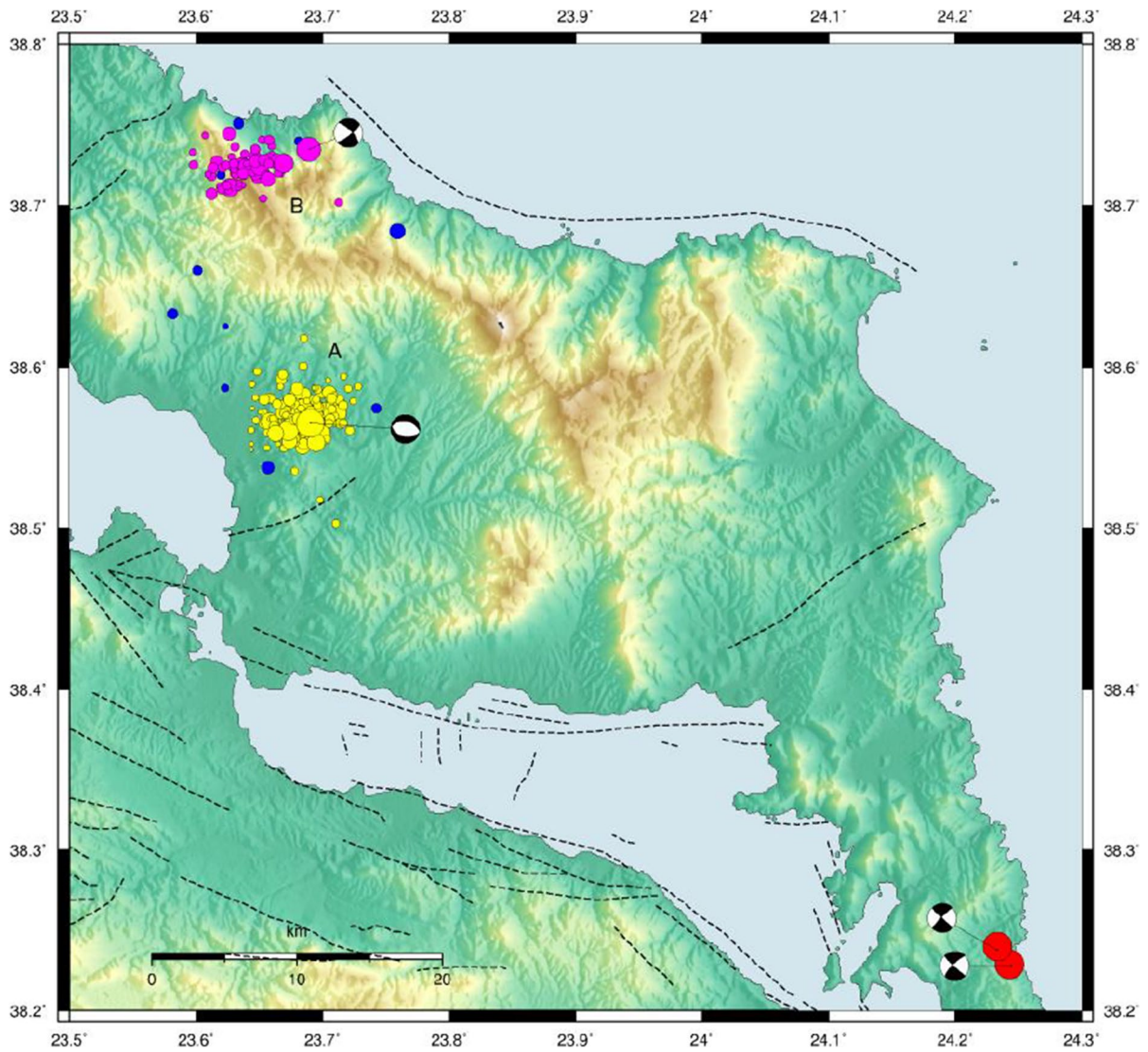


Fig. 10 Relief Map of south and central Evia showing the distribution of the events which occurred in triggered areas A and B, two months before (blue circles) and two months after

(A, yellow and B, magenta circles) the South Evia main events (red circles). Beach balls show focal mechanisms of events (black color indicates compressional quadrants)

Gomberg and Johnson (2005) had shown that after an earthquake not only numerous smaller shocks are triggered, over distances comparable to the dimensions of the mainshock fault rupture, but it can cause further earthquakes at any distance, if their amplitude exceeds several microstrain, regardless of their frequency content. Their results were confirmed by laboratory measurements of modulus reduction against dynamic loading strain amplitude for various rock types, pressures, and saturations.

Initially, in order to detect any indication of possible seismicity rate changes, we performed two statistical tests. The β -statistic (Matthews and Reasenberg 1988) is a measure of the difference between the number of events that occur versus the expected number of events normalized by the standard deviation:

$$\beta = \frac{N_a - \Lambda}{\sqrt{\Lambda}}$$

where $\Lambda = N_b \times \frac{t_a}{t_b}$, N_b , and N_a are the number of earthquakes before and after the stressing event (29 November 2022 events), respectively, and t_b and t_a are the time window lengths before and after, respectively. A $\beta \geq 2.0$ indicates a change in seismicity with 95% significance. The Z-statistic (Habermann 1987) defines the difference between the mean rate of seismicity in the period before and after the stressing event as

$$Z = \frac{\frac{N_a}{\Delta t_a} - \frac{N_b}{\Delta t_b}}{\sqrt{\frac{N_a}{\Delta t_a^2} + \frac{N_b}{\Delta t_b^2}}}$$

$Z \sim 2$ indicates 95% significance; thus, to indicate a change in the seismicity rate, we use a threshold of $Z \geq 2.0$ (Pena Castro et al. 2019).

We considered $t_b = t_a$ set to 60 days and we investigated the sequences, which took place afterwards in central Evia, independently (Fig. 10). The results are $\beta_A=30$ and $\beta_B=62.7$ while $Z_A = 7.3$ and $Z_B = 12.4$. Since $\beta > 2.0$ and $Z > 2.0$ for both activated areas, A and B, there is a certain indication of change in the seismicity rate which occurred during the November–December 2022 period (Fig. S13). Moreover, significant triggered rate changes implying dynamic triggering, has been observed in regions with geothermal activity (Gomberg et al. 2003; Brodsky 2006), a characteristic that may be found also in this case as central-north Evia is characterized by a shallow geothermal system in interaction with the local fault systems, both onshore and offshore (Palyvos et al. 2006; Karastathis et al. 2011; Kanellopoulos et al. 2016, 2020; Caroir et al. 2023). Consequently, we investigate the possibility of delayed dynamic stress triggering of the central Evia December 2022 events (areas A and B; Fig. 10) by the South Evia November 2022 major events.

When earthquake rupture propagates in a preferential direction (Haskell 1964), the ground motions in that direction can be greatly amplified and such a rupture directivity effect is frequently observed in not only large but also many moderate. In the case of L'Aquila2009 earthquake, Convertito et al. (2013) observed that for each main earthquake its aftershocks and the subsequent main events occur in the areas oriented as the source dominant rupture direction.

We measured the horizontal component of the seismic waves' peak ground-motion velocity (PGV; Fig. 11) recorded at distances up to 280 km from the 29 November 2022 events (with magnitude, M_w , of 4.6 to 4.8); at each station, the PGV corresponds to the largest value between the two horizontal components of the recorded velocity. Figures 11 (a and b) show the map distribution of the PGV values for both events; a pattern of PGV values distribution can be identified, while largest values appear in a direction NNW-SSE, parallel to the fault rupture (see yellow line in Fig. 9). In the region of central Evia (Fig. 11), for both events, the PGVs approximate 0.4 cm/s that is expected to dynamically trigger faults at distances 60–80 km (Gomberg and Johnson 2005). Previous studies (Gomberger et al. 2003) also have noted the influence of the rupture direction in the dynamic stress field for large and small-to-moderate earthquakes, expecting the greatest correlation for strike-slip events because the rupture propagation direction corresponds to maxima in the shear wave radiation pattern. In the near field, S waves should carry the largest dynamic strains (Boatwright et al. 2001) and PGV approximates the peak shear strain when divided by the shear wave velocity (Kanamori and Brodsky 2004). Peak dynamic strain is roughly proportional to the amplitude of seismic waves

$$\varepsilon \approx \frac{A}{\Lambda} \approx \frac{V}{C_s}$$

where A is displacement amplitude, Λ is wavelength, V is particle velocity, and C_s is seismic wave velocity (Love 1927). Assuming radial symmetry (i.e., approximating the trigger as a point source), the peak dynamic strain in the near-field disk could be estimated as:

$$\varepsilon = \frac{PGV}{C_s}$$

where C_s is shear wave velocity and PGV is the peak ground velocity (van der Elst and Brodsky 2010). The velocity C_s refers to the depth of the hypocenter of the main source. This direct comparison of strain with velocity can highlight physical path effects (Farghal et al. 2020). The distribution of the peak PGV values (Fig. 11) indicates that the December 2022 seismicity rate in central Evia (areas A and B in Fig. 10) could be affected by the South Evia sequence. Peak

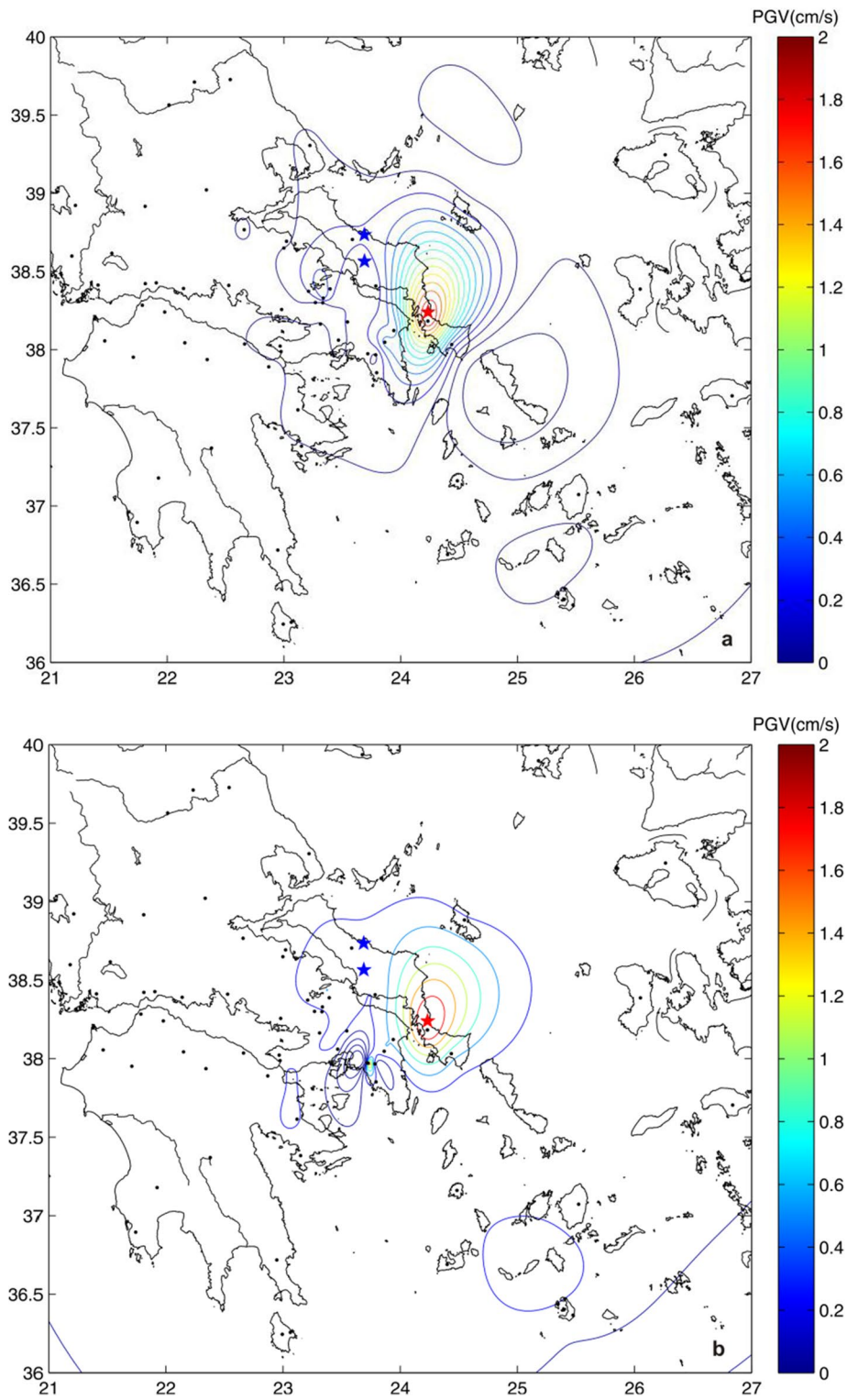


Fig. 11 Maps showing the peak ground velocity (PGV) distribution for the event of 29 November 2022 04:32 UTC (a) and for the event of 29 November 2022 20:06 UTC (b), presented

as red stars. The December 2022 events that were possibly triggered afterwards in central Evia appear with blue stars

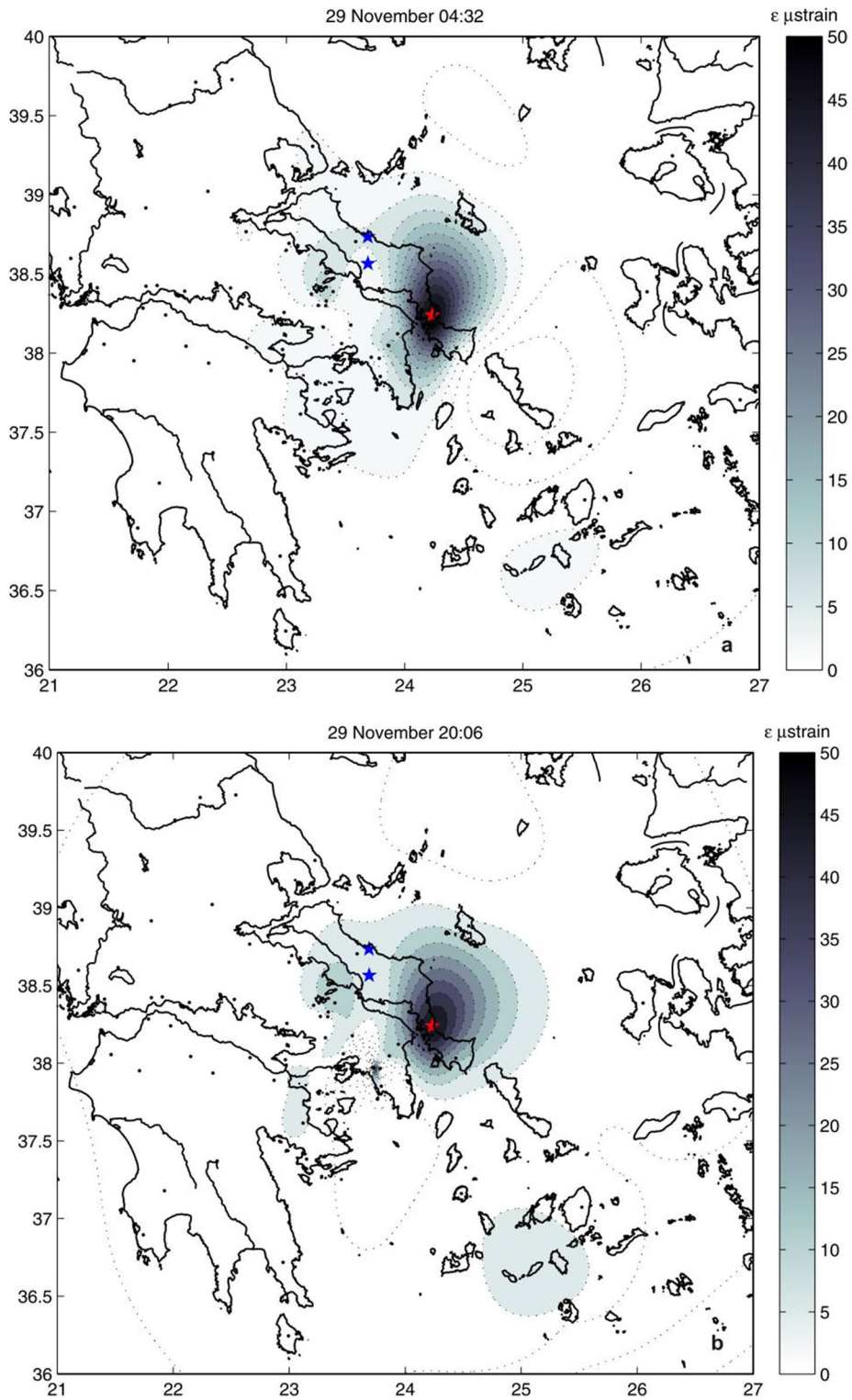


Fig. 12 Maps showing the peak dynamic strain (PDS) field obtained using PGV as a proxy calculated for **a** event of 29 November 2022 04:32 UTC and **b** event of 29 November 2022

20:06 UTC (red stars). The December 2022 events that were possibly triggered in central Evia appear with blue stars

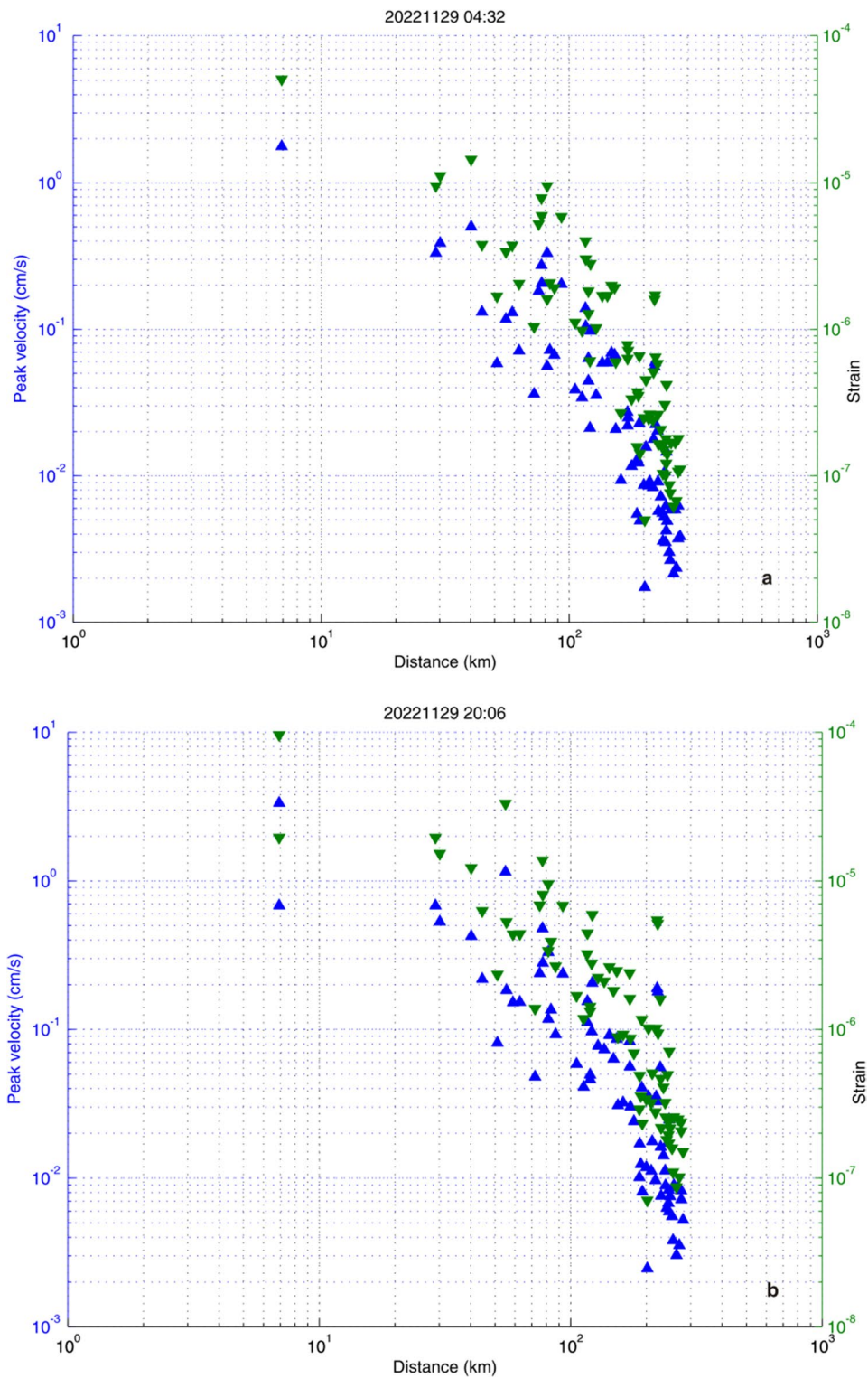


Fig. 13 Plot of measured peak ground velocity (PGVs, blue triangles; data from the NOA EIDA node) and strain (green triangles) against distance normalized by rupture dimensions for

two main events of the sequence; **a** the event of 29 November 2022, 04:32 and **b** the event of 29 November 2022, 20:06

dynamic strains range between 8 and 14 μ strain (Fig. 12).

Moreover, we calculated the measured peak ground-motion velocity (PGV, which approximates the peak shear strain when divided by the shear wave or phase velocity) at distances normalized by rupture dimensions, using the square root of the rupture area (same area as in the Coulomb stress change calculations in section 4.1) as suggested by Gomberg and Johnson (2005). Evidence presented by Gomberg et al. (2001) imply that transient dynamic deformations could trigger earthquakes, although the mechanism(s) by which they do so remain unknown, while the thresholds span a small range from between 0.1 cm/s to a few tens of cm/s and around 30 micro-strain (μ s). Our observations (Fig. 13) indicate that dynamic triggering of the central Evia earthquakes might be possible.

In many cases triggering of earthquakes occurs within minutes to hours following the passage of the seismic waves (Brodsky et al. 2000; Fan et al. 2021), yet in other cases, earthquakes occurring weeks to months after the initial earthquake have been interpreted as delayed response to dynamic triggering (Hough 2005; Brodsky 2006; Parsons et al. 2014). Delayed triggered responses may reflect more complex series of physical processes and may trigger an aseismic process such as fault creep (Prejean and Hill 2009). Moreover, De Barros et al. (2017) found that regional earthquakes originating from azimuths between N340° and N80° with respect to the E-W trending Gulf of Corinth rift lead to dynamic triggering, whatever the distance or the wave amplitude. De Barros et al. (2017) suggested that earthquakes of smaller magnitudes also have the potential to trigger remote seismicity, while more delayed triggering might involve fluid diffusion (even the very small perturbations from remote $M_w=4.5$ earthquakes allow for a pressurization of interstitial fluids and an increase of seismicity). The December 2022–January 2023 (triggered) seismicity on central Evia occurred on an E-W striking normal fault zone (Psachna; Benetatos et al. 2004) and on N51°E (NOA solution) striking right-lateral strike-slip fault (Vlahia), respectively. We note that these faults are located to the NW of the November 2022 source events or in terms of azimuth they are oriented N300°E–N320°E with respect to the location of the triggering source. Moreover, the azimuthal location of the triggered events is

nearly co-planar to the NW-SE orientation of the 29 November 2022 left-lateral, strike-slip fault, implying a possible directivity effect. Therefore, the delayed triggering (~ 30 days) of the central Evia events is not unexpected and may be explained by secondary triggering mechanisms initiated by dynamic stresses, such as fluid migration (De Barros et al. 2017). The upper crust of central and North Evia hosts geothermal fluids (e.g., Karastathis et al. 2011; Kanellopoulos et al. 2016, 2020) and transient, dynamic strains (Fig. 12) can induce transient changes in pressure. However, we note that quantifying the connection between earthquakes and delayed triggered seismic sequences at distances more than 2–3 rupture lengths is much more challenging.

6 Conclusions

We investigated the seismicity patterns preceding, during and following the 29 November 2022 events onshore South Evia, central Greece. The main findings can be summarized as follows:

- The 29 November 2022 events ruptured a blind, near-vertical left-lateral strike slip fault striking NW-SE.
- The fault plane is projected onshore South Evia southeast of village Almyropotamos.
- The main events were preceded by a 35-day foreshock sequence that occurred in two groups with most events concentrated within 1-km from the epicenter of the 29 November 2022 04:32 UTC.
- The frequency-magnitude distribution of the foreshocks is notably different than the post-mainshock sequence as the foreshock b -value = 1.37 vs. 0.78 of the latter.
- The static stress transfer modeling indicated that stress loading on nearby faults diminishes below 0.1 bar at distances larger than 7 km from the mainshock.
- The cumulative loading of the area SE of the epicenter of $M_w=4.8$ event (29 November 2022 20:06 UTC) reached stress levels which explain the occurrence of aftershocks for several months (end of April 2023).
- The map distribution of computed PGVs and peak dynamic strains indicates local maxima in central

Evia (Psachna and Vlahia regions) where two seismic sequences occurred in late December 2022–early January 2023.

- The December 2022 sequences in central Evia possibly occurred because of delayed dynamic stress triggering due to the existence of geothermal fluids and the NW-SE strike (directivity effect) of the November 2022 seismic fault.

Author contributions A.S. and A.G. made substantial contributions to the Conceptualization, Methodology, Formal Analysis, Investigation, Visualization, Writing-Original Draft, Review and Editing. All authors read and approved the final manuscript.

Funding Open access funding provided by HEAL-Link Greece.

Data availability Data from seismometers and accelerometers can be retrieved from European Plate Observing System (EPOS) nodes (<https://www.orfeus-eu.org/data/eida/nodes/>), European Integrated Data Archive (EIDA) nodes at RESIF, and National Observatory of Athens (NOA; Evangelidis et al., 2021). Phase and focal mechanism data of GI-NOA at <http://bbnet.gein.noa.gr/HL/databases/database>. Catalog and phase data are acquired from the following regional networks: HUSN (HL, doi: <https://doi.org/10.7914/SN/HL>); HT, doi: <https://doi.org/10.7914/SN/HT>); HA, doi: <https://doi.org/10.7914/SN/HA>); HP, doi: <https://doi.org/10.7914/SN/HP>); HI, doi: <https://doi.org/10.7914/SN/Hi>); HC, doi: <https://doi.org/10.7914/SN/HC>); and data from station GR27 of AdriaArray Temporary Network, 1Y, doi: <https://doi.org/10.7914/y0t2-3b67>).

Declarations

Competing interests The authors declare no competing interests.

Open Access This article is licensed under a Creative Commons Attribution 4.0 International License, which permits use, sharing, adaptation, distribution and reproduction in any medium or format, as long as you give appropriate credit to the original author(s) and the source, provide a link to the Creative Commons licence, and indicate if changes were made. The images or other third party material in this article are included in the article's Creative Commons licence, unless indicated otherwise in a credit line to the material. If material is not included in the article's Creative Commons licence and your intended use is not permitted by statutory regulation or exceeds the permitted use, you will need to obtain permission directly from the copyright holder. To view a copy of this licence, visit <http://creativecommons.org/licenses/by/4.0/>.

References

- Ambraseys NN, Jackson JA (1990) Seismicity and associated strain of central Greece between 1890 and 1988. *Geophys J Int* 101(3):663–708
- Atzori S, Manunta M, Fornaro G, Ganas A, Salvi S (2008) Postseismic displacement of the 1999 Athens earthquake retrieved by the Differential Interferometry by Synthetic Aperture Radar time series. *J Geophys Res* 113:B09309. <https://doi.org/10.1029/2007JB005504>
- Benetatos C, Kiratzi A, Kementzetzidou K, Roumelioti Z, Karakaisis G, Scordilis E, Latoussakis I, Drakatos G (2004) The Psachna (Evia Island) earthquake swarm of June 2003. *Bull Geol Soc Greece* 36(3):1379–1388
- Boatwright J, Thywissen K, Seekins LC (2001) Correlation of ground motion and intensity for the 17 January 1994 Northridge, California, earthquake. *Bull Seismol Soc Am* 91(4):739–752
- Bouchon M (1981) A simple method to calculate Green's functions for elastic layered media. *Bull Seismol Soc Am* 71:959–971
- Briole P, Ganas A, Elias P, Dimitrov D (2021) The GPS velocity field of the Aegean. New observations, contribution of the earthquakes, crustal blocks model. *Geophys J Int* 226(1):468–492. <https://doi.org/10.1093/gji/ggab089>
- Brodsky EE (2006) Long-range triggered earthquakes that continue after the wave train passes. *Geophys Res Lett* 33:L15313. <https://doi.org/10.1029/2006GL026605>
- Brodsky EE, Karakostas V, Kanamori H (2000) A new observation of dynamically triggered regional seismicity: earthquakes in Greece following the August 1999 Izmit, Turkey earthquake. *Geophys Res Lett* 27(17):2741–2744. <https://doi.org/10.1029/2000GL011534>
- Caroir F et al (2023) Late Quaternary deformation in the western extension of the North Anatolian Fault (North Evia, Greece): insights from very high-resolution seismic data (WATER surveys). *Tectonophysics*:230138. <https://doi.org/10.1016/j.tecto.2023.230138>
- Chatzipetros A, Kiratzi A, Sboras S, Zouros N, Pavlides S (2013) Active faulting in the north-eastern Aegean Sea Islands. *Tectonophysics* 597–598:106–122. <https://doi.org/10.1016/j.tecto.2012.11.026>
- Chousianitis K, Ganas A, Evangelidis CP (2015) Strain and rotation rate patterns of mainland Greece from continuous GPS data and comparison between seismic and geodetic moment release. *J Geophys Res Solid Earth* 120:3909–3931. <https://doi.org/10.1002/2014JB011762>
- Chousianitis K, Ganas A, Gianniu M (2013) Kinematic interpretation of present-day crustal deformation in central Greece from continuous GPS measurements. *J Geodyn* 71:1–13. <https://doi.org/10.1016/j.jog.2013.06.004>
- Convertito V, Catalli F, Emolo A (2013) Combining stress transfer and source directivity: the case of the 2012 Emilia seismic sequence. *Sci Rep* 3:3114. <https://doi.org/10.1038/srep03114>
- Cundy AB, Gaki-Papanastassiou K, Papanastassiou D, Maroukian H, Frogley MR, Cane T (2010) Geological and geomorphological evidence of recent coastal uplift along a major Hellenic normal fault system (the

- Kamena Vourla fault zone, NW Evoikos Gulf, Greece). *Mar Geol* 271:156–164
- D'Agostino N, Cheloni D, Fornaro G, Giuliani R, Reale D (2012) Space-time distribution of afterslip following the 2009 L'Aquila earthquake. *J Geophys Res* 117:B02402. <https://doi.org/10.1029/2011JB008523>
- D'Agostino N, Métois M, Koci R, Duni L, Kuka N, Ganas A, Georgiev I, Jouanne F, Kaludjerovic N, Kandić R (2020) Active crustal deformation and rotations in the southwestern Balkans from continuous GPS measurements. *Earth Planet Sci Lett* 539:116246. <https://doi.org/10.1016/j.epsl.2020.116246>
- De Barros L, Deschamps A, Sladen A, Lyon Caen H, Voulgaris N (2017) Investigating dynamic triggering of seismicity by regional earthquakes: the case of the Corinth rift (Greece). *Geophys Res Lett* 44. <https://doi.org/10.1002/2017gl075460>
- Deligiannakis G, Papanikolaou ID, Roberts G (2018) Fault specific GIS based seismic hazard maps for the Attica region, Greece. *Geomorphology* 306:264–282. <https://doi.org/10.1016/j.geomorph.2016.12.005>
- Efron B (1982) The jackknife, the bootstrap, and other resampling plans. SIAM, Philadelphia, p 92
- Ellsworth WL, Bulut F (2018) Nucleation of the 1999 Izmit earthquake by a triggered cascade of foreshocks. *Nat Geosci* 11:531–535
- Evangelidis C, Fountoulakis I (2023) Imaging the western edge of the Aegean shear zone: the South Evia 2022–2023 seismic sequence. *Seismica* 2(1). <https://doi.org/10.26443/seismica.v2i1.1032>
- Evelpidou N, Vassilopoulos A, Pirazzoli P (2011) Holocene emergence in Euboea island (Greece). *Mar Geol* 295–298:14–19
- Fan W, Barbour AJ, Cochran ES, Lin G (2021) Characteristics of frequent dynamic triggering of microearthquakes in Southern California. *J Geophys Res Solid Earth* 126:e2020JB020820. <https://doi.org/10.1029/2020JB020820>
- Farghal N, Baltay A, Langbein J (2020) Strain-estimated ground motions associated with recent earthquakes in California. *Bull Seismol Soc Am* 110. <https://doi.org/10.1785/0120200131>
- Freed AM (2005) Earthquake Triggering by Static, Dynamic, and Postseismic Stress Transfer. *Annu Rev Earth Planet Sci* 33:335–367. <https://doi.org/10.1146/annurev.earth.33.092203.122505>
- Ganas A, Drakatos G, Pavlides SB, Stavrakakis GN, Ziazia M, Sokos E, Karastathis VK (2005) The 2001 $M_w = 6.4$ Skyros earthquake, conjugate strike-slip faulting and spatial variation in stress within the central Aegean Sea. *J Geodyn* 39:61–77
- Ganas A, Mouzakiotis E, Moshou A, Karastathis V (2016) Left-lateral shear inside the North Gulf of Evia Rift, Central Greece, evidenced by relocated earthquake sequences and moment tensor inversion. *Tectonophysics* 682:237–248. <https://doi.org/10.1016/j.tecto.2016.05.031>
- Ganas A, Oikonomou IA, Tsimi Ch (2013) NOA faults: a digital database for active faults in Greece. *Geol Soc Greece* 47(2):518–530. <https://doi.org/10.12681/bgsg.11079>
- Ganas A, Roumelioti Z, Karastathis V, Chousianitis K, Moshou A, Mouzakiotis A (2014) The Lemnos 8 January 2013 ($M_w = 5.7$) earthquake: fault slip, aftershock properties and static stress transfer modeling in the north Aegean Sea. *J Seismol* 18, (3):433–455. <https://doi.org/10.1007/s10950-014-9418-3>
- Ganas A, Sokos E, Agalos A, Leontakianakos G, Pavlides S (2006) Coulomb stress triggering of earthquakes along the Atalanti Fault, central Greece: two April 1894 M_6+ events and stress change patterns. *Tectonophysics* 420:357–369
- Ganas, A.; Tsironi, V.; Efstathiou, E.; Konstantakopoulou, E.; Andritsou, N.; Georgakopoulos, V.; Tsimi, C.; Fokaefs, A.; Madonis, N. (2023) The National Observatory of Athens active faults of Greece database (NOAFAULTs), Version 2023. In *Past Earthquakes and Advances in Seismology for Informed Risk Decision-Making, Book of Abstracts, Proceedings of the 8th International Colloquium on Historical Earthquakes, Palaeo—Macroseismology and Seismotectonics; Special Publication; Bulletin of the Geological Society of Greece: Athens, Greece, 2023; pp. 36–38. ISBN 978-618-86841-1-9.*
- Goldsworthy M, Jackson J, Haines J (2002) The continuity of active fault systems in Greece. *Geophys J Int* 148(3):596–618. <https://doi.org/10.1046/j.1365-246X.2002.01609.x>
- Gomberg J, Bodin P, Reasenber PA (2003) Observing earthquakes triggered in the near field by dynamic deformations. *Bull Seismol Soc Am* 93(1):118–138
- Gomberg J, Johnson P (2005) Dynamic triggering of earthquakes. *Nature* 437:830. <https://doi.org/10.1038/437830a>
- Gomberg J, Reasenber PA, Bodin P, Harris RA (2001) Earthquake triggering by seismic waves following the Landers and Hector Mine earthquakes. *Nature* 411:462–466. <https://doi.org/10.1038/35078053>
- Grützner C, Schneiderwind S, Papanikolaou I, Deligiannakis G, Pallikarakis A, Reicherter K (2016) New constraints on extensional tectonics and seismic hazard in northern Attica, Greece: the case of the Milesi Fault. *Geophys J Int* 204(1):180–199. <https://doi.org/10.1093/gji/ggv443>
- Habermann RE (1987) Man-made changes of seismicity rates. *Bull Seismol Soc Am* 77(1):141–159. <https://doi.org/10.1785/BSSA0770010141>
- Harris RA, Simpson RW (1998) Suppression of large earthquakes by stress shadows: a comparison of Coulomb and rate and state failure. *J Geophys Res* 103:439–451
- Haskell NA (1964) Total energy and energy spectral density of elastic wave radiation from propagating faults. *Bull Seismol Soc Am* 54(6A):1811–1841. <https://doi.org/10.1785/BSSA05406A1811>
- Hough SE (2005) Remotely triggered earthquakes following moderate mainshocks (or why California is not falling into the ocean). *Seismol Res Lett* 76:58–66
- Hurter S, Schellschmidt R (2003) Atlas of geothermal resources in Europe. *Geothermics* 32(4–6):779–787
- Iezzi F, Roberts G, Faure Walker J, Papanikolaou I, Ganas A et al (2021) Temporal and spatial earthquake clustering revealed through comparison of millennial strain-rates from ^{36}Cl cosmogenic exposure dating and decadal GPS strain-rate. *Sci Rep* 11:23320. <https://doi.org/10.1038/s41598-021-02131-3>
- IGME (1991) Geological map 1:50,000 series “Rafina Sheet”
- Kagan YY (2004) Short term properties of earthquake catalogs and models of earthquake source. *Bull Seismol Soc Am* 94(4):1207–1228

- Kanamori, H., Brodsky, E.E. (2004) The physics of earthquakes. *Rep Prog Phys* 67 (8). <https://doi.org/10.1088/0034-4885/67/8/R03> pii: S0034-4885(04)25227-7.
- Kanellopoulos C, Christopoulou M, Xenakis M, Vakalopoulos P (2016) Hydrochemical characteristics and geothermometry applications of hot groundwater in Edipos area, NW Euboea (Evia), Greece. *Bull Geol Soc Greece* 50(2):720–729. <https://doi.org/10.12681/bgsg.11778>
- Kanellopoulos C, Xenakis M, Vakalopoulos P et al (2020) Seawater-dominated, tectonically controlled and volcanic related geothermal systems: the case of the geothermal area in the northwest of the island of Euboea (Evia), Greece. *Int J Earth Sci (GeolRundsch)* 109:2081–2112. <https://doi.org/10.1007/s00531-020-01889-7>
- Karakostas V, Papadimitriou E, Gospodinov D (2014) Modelling the 2013 North Aegean (Greece) seismic sequence: geometrical and frictional constraints, and aftershock probabilities. *Geophys J Int* 197(1):525–541. <https://doi.org/10.1093/gji/ggt523>
- Karakostas VG, Papadimitriou EE, Karakaisis GF, Papazachos CB, Scordilis EM, Vargemezis G, Aidona E (2003) The 2001 Skyros, Northern Aegean, Greece, earthquake sequence: off – fault aftershocks, tectonic implications, and seismicity triggering. *Geophys Res Lett* 30(1):1012. <https://doi.org/10.1029/2002GL015814>
- Karastathis V, Papoulia J, Di Fiore B, Makris J, Tsambas A, Stampolidis A, Papadopoulos G (2011) Deep structure investigations of the geothermal field of the North Euboean Gulf, Greece, using 3-D local earthquake tomography and Curie Point Depth analysis. *J Volcanol Geotherm Res* 206:106–120
- Karytsas S, Polyzou O, Karytsas C (2019) Social aspects of geothermal energy in Greece. In: *Geothermal Energy and Society*. Springer, Cham, Switzerland, pp 123–144
- Kassaras I, Kapetanidis V, Ganas A, Karakonstantis A, Papadimitriou P, Kaviris G, Kouskouna V, Voulgaris N (2022) Seismotectonic analysis of the 2021 Damasi-Tyrnavos (Thessaly, Central Greece) earthquake sequence and implications on the stress field rotations. *J Geodyn* 150:101898. <https://doi.org/10.1016/j.jog.2022.101898>
- Kaviris G, Papadimitriou P, Makropoulos K (2007) Magnitude scales in central Greece. *Bull Geol Soc Greece* 40(3):1114–1124. <https://doi.org/10.12681/bgsg.16838>
- Kaviris G, Spingos I, Millas C, Kapetanidis V, Fountoulakis I, Papadimitriou P et al (2018) Effects of the January 2018 seismic sequence on shear-wave splitting in the upper crust of Marathon (NE Attica, Greece). *Phys Earth Planet Inter* 285:45–58
- Kavouridis T, Papadeas G (1990) Results of geothermal research in the region “Lilantio Plain” (Prefecture of Evia). Institute of Geological and Mineral Exploration, Athens, p 13 Technical Report, (in Greek)
- Klein FW (2002) User’s guide to HYPOINVERSE-2000: a Fortran program to solve for earthquake locations and magnitudes. *US Geol Surv Prof Pap Rep* 02-17:1–123
- Kokkalas S (2001) Tectonic evolution and stress field of the Kymi-Aliveri basin, Evia island, Greece. *Bull Geol Soc Greece* 34(1):243–249. <https://doi.org/10.12681/bgsg.17019>
- Kolínský, P., Meier, T. and Seismic Network Working Group, T A (2022) Status and Implementation of the AdriaArray Seismic Network, EGU General Assembly 2022, Vienna, Austria, 23–27 May 2022, EGU22-E7246, <https://doi.org/10.5194/egusphere-egu22-7246>,
- Konstantinou K, Mouslopoulou V, Saltogianni V (2020) Seismicity and active faulting around the metropolitan area of Athens, Greece. *Bull Seismol Soc Am* 110:1924–1941. <https://doi.org/10.1785/0120200039>
- Konstantinou KI (2018) Estimation of optimum velocity model and precise earthquake locations in NE Aegean: implications for seismotectonics and seismic hazard. *J Geodyn* 121:143–154. <https://doi.org/10.1016/j.jog.2018.07.005>
- Lin J, Stein RS (2004) Stress triggering in thrust and subduction earthquakes, and stress interaction between the southern San Andreas and nearby thrust and strike-slip faults. *J Geophys Res* 109:B02303. <https://doi.org/10.1029/2003JB002607>
- Love AEH (1927) *Mathematical theory of elasticity*. Cambridge Univ, Cambridge, U. K.
- Matthews MV, Reasenber PA (1988) Statistical methods for investigating quiescence and other temporal seismicity patterns. *PAGEOPH* 126:357–372. <https://doi.org/10.1007/BF00879003>
- Mettos A, Rontogianni T, Papadakis G, Paschos P, Georgiou C (1991) New data on the geology of the Neogene deposits of the North Euboea. *Bull Geol Soc Greece* 25:71–83
- Mignan A, Werner MJ, Wiemer S, Chen CC, Wu YM (2011) Bayesian estimation of the spatially varying completeness magnitude of earthquake catalogs. *Bull Seismol Soc Am* 101(3):1371–1385
- Mouzakiotis A, Karastathis V (2016) Improved earthquake location in the area of North Euboean Gulf after the implementation of a 3D non-linear location method in combination with a 3D velocity model. *Bull Geol Soc Greece* 47:1185. <https://doi.org/10.12681/bgsg.10974>
- Okada Y (1992) Internal deformation due to shear and tensile faults in a half-space. *Bull Seismol Soc Am* 82:1018–1040
- Olasoglou E, Tsapanos T, Papadimitriou E, Drakatos G (2016) Some preliminary results on the distribution of the aftershock sequences in Japan - Kuril Islands and Kamchatka. *Bull Geol Soc Greece* 50(3)
- Palyvos N, Bantekas J, Kranis H (2006) Transverse fault zones of subtle geomorphic signature in Northern Evia island (Central Greece extensional province): an introduction to the Quaternary Nileas graben. *Geomorphology* 76(3-4):363–374. <https://doi.org/10.1016/j.geomorph.2005.12.002>
- Papadopoulos G, Ganas A, Plessa A (2002) The Skyros earthquake (Mw6.5) of 26 July 2001 and precursory seismicity patterns in the North Aegean Sea. *Bull Seismol Soc Am* 92(30):1141–1145
- Papadopoulos GA, Drakatos G, Plessa A (2000) Foreshock activity as a precursor of strong earthquakes in Corinthos Gulf, Central Greece. *Phys Chem Earth Solid Earth Geod* 25(3):239–245. [https://doi.org/10.1016/S1464-1895\(00\)00039-9](https://doi.org/10.1016/S1464-1895(00)00039-9)
- Papanikolaou D, Lykousis V, Chronis G, Pavlakis P (1988) A comparative study of neotectonic basins across the Hellenic arc: the Messiniakos, Argolikos, Saronikos and

- Southern Evoikos Gulfs. *Basin Res* 1:167–176. <https://doi.org/10.1111/j.1365-2117.1988.tb00013.x>
- Papanikolaou D, Nomikou P, Papanikolaou I, Lampridou D, Rousakis G, Alexandri M (2019) Active tectonics and seismic hazard in Skyros Basin, North Aegean Sea, Greece. *Mar Geol* 407:94–110
- Papazachos B, Papazachou C (1997) The earthquakes of Greece. Ziti editions, Thessaloniki
- Papoulia J, Makris J, Drakopoulou V (2006) Local seismic array observations at north Evoikos, central Greece, delineate crustal deformation between the North Aegean Trough and Corinthiakos Rift. *Tectonophysics* 423(1–4):97–106
- Parsons T, Segou M, Marzocchi W (2014) The global after-shock zone. *Tectonophysics* 618:1–34
- Pena Castro AF, Dougherty SL, Harrington RM, Cochran ES (2019) Delayed dynamic triggering of disposal-induced earthquakes observed by a dense array in northern Oklahoma. *J Geophys Res Solid Earth* 124:3766–3781. <https://doi.org/10.1029/2018JB017150>
- Perissoratis C, Van Andel TH (1991) Sealevel changes and tectonics in the Quaternary extensional basin of the South Evvoikos Gulf, Greece. *Terra Nova* 3(3):294–302
- Pirazzoli PA, Stiros SC, Arnold M, Laborel J, Laborel-Deguen F (1999) Late Holocene coseismic vertical displacement and tsunami deposits near Kynos, Gulf of Euboea, central Greece. *Phys Chem Earth* 24:361–367
- Prejean SG, Hill DP (2009) Earthquakes, dynamic triggering of. In: Meyers R (ed) *Encyclopedia of Complexity and Systems Science*. Springer, New York, NY. https://doi.org/10.1007/978-0-387-30440-3_157
- Reasenber PA, Simpson RW (1992) Response of regional seismicity to the static stress change produced by Loma Prieta earthquake. *Science* 255:1687–1690
- Roberts GP, Ganas A (2000) Fault-slip directions in central and southern Greece measured from striated and corrugated fault planes: comparison with focal mechanism and geodetic data. *J Geophys Res* 105:23443–23462
- Roberts S, Jackson J (1991) Active normal faulting in central Greece: an overview. *Geol Soc Lond, Spec Publ* 56:125–142
- Rondoyanni T, Galanakis D, Georgiou C, Baskoutas I (2007) Identifying fault activity in the central Evoikos gulf (Greece). *Bull Geol Soc Greece* 40(1):439–450. <https://doi.org/10.12681/bgsg.16639>
- Rydelek P, Sacks I (1989) Testing the completeness of earthquake catalogues and the hypothesis of self-similarity. *Nature* 337:251–253. <https://doi.org/10.1038/337251a0>
- Sakellariou D, Rousakis G, Kaberi H, Kapsimalis V, Georgiou P, Kanellopoulos T, Lykousis V (2007) Tectono-sedimentary structure and late Quaternary evolution of the north Evia gulf basin, central Greece: preliminary results. *Bull Geol Soc Greece* 40(1):451–462. <https://doi.org/10.12681/bgsg.16644>
- Scholz CH (1968) Frequency-magnitude relation of microfracturing in rock and its relation to earthquakes. *Bull Seismol Soc Am* 58(1):399
- Sokos E, Zahradnik J (2008) ISOLA a Fortran code and a Matlab GUI to perform multiple-point source inversion of seismic data. *Comput Geosci* 34:967–977. <https://doi.org/10.1016/j.cageo.2007.07.005>
- Sokos E, Zahradnik J (2013) Evaluating centroid-moment-tensor uncertainty in the new version of ISOLA software. *Seismol Res Lett* 84:656–665. <https://doi.org/10.1785/0220130002>
- Stiros SC, Arnold M, Pirazzoli PA, Laborel J, Laborel F, Papa-georgiou S (1992) Historical coseismic uplift on Euboea island, Greece. *Earth Planet Sci Lett* 108(1–3):109–117
- Tombros SF, Kokkalas S, Seymour KS et al (2021) The Kallianos Au-Ag-Te mineralization, Evia Island, Greece: a detachment-related distal hydrothermal deposit of the Attico-Cycladic Metallogenic Massif. *Mineral Deposita* 56:665–684. <https://doi.org/10.1007/s00126-020-00989-3>
- Valkaniotis S, De Novellis V, Ganas A et al (2023) The 2 December 2020 MW 4.6, Kallithea (Viotia), central Greece earthquake: a very shallow damaging rupture detected by InSAR and its role in strain accommodation by neotectonic normal faults. *Acta Geophys.* <https://doi.org/10.1007/s11600-023-01213-2>
- Valkanou K, Karymbalis E, Papanastassiou D, Soldati M, Chalkias C, Gaki-Papanastassiou K (2021) Assessment of neotectonic landscape deformation in Evia Island, Greece, using GIS-based multi-criteria analysis. *ISPRS Int J Geo Inf* 10(3):118. <https://doi.org/10.3390/ijgi10030118>
- van der Elst NJ, Brodsky EE (2010) Connecting near-field and far-field earthquake triggering to dynamic strain. *J Geophys Res* 115:B07311. <https://doi.org/10.1029/2009JB006681>
- Waldhauser F (2001) hypoDD-A program to compute double-difference hypocenter locations, U.S. Geol Surv Open File Rep 01-113:25
- Waldhauser F, Ellsworth W (2000) A double-difference earthquake location algorithm: method and application to the northern Hayward fault, California. *Bull Seismol Soc Am* 90:1353–1368. <https://doi.org/10.1785/0120000006>
- Wells DL, Coppersmith KJ (1994) New empirical relationships among magnitude, rupture length, rupture width, rupture area, and surface displacement. *Bull Seismol Soc Am* 84(4):974–1002
- Wiemer S (2001) A Software Package to Analyze Seismicity: ZMAP. *Seismol Res Lett* 72:373–382
- Wiemer S, Wyss M (2000) Minimum magnitude of completeness in earthquake catalogs: examples from Alaska, the Western United States, and Japan. *Bull Seismol Soc Am* 90:859–869
- Zahradnik J, Sokos E (2018) ISOLA code for multiple-point source modeling—review, in *Moment Tensor Solutions* Sebastian D’Amico (Editor). Springer, Cham, pp 1–28. https://doi.org/10.1007/978-3-319-77359-9_1
- Zahradnik J, Gallovič F, Sokos E, Serpetsidaki A, Tselentis A (2008) Quick fault-plane identification by a geometrical method: application to the MW 6.2 Leonidio Earthquake, 6 January 2008, Greece. *Seismol Res Lett* 79:653–662. <https://doi.org/10.1785/gssrl.79.5.653>

Publisher’s Note Springer Nature remains neutral with regard to jurisdictional claims in published maps and institutional affiliations.